A Szilikátipari Tudományos Egyesület lapja

építőanyag

Journal of Silicate Based and Composite Materials

A TARTALOMBÓL:

2022/6

Invitation to CMCEE-14

The 14th International Conference on Ceramic Materials and Components for Energy and Environmental Applications (CMCEE-14) will be held in the beautiful city of Budapest, Hungary. The conference series began in 1980s and has established a strong reputation for state-of-the-art presentations and information exchange on the latest emerging ceramic technologies and their wide ranging applications. CMCEE-14 will contain more than 30 symposia covering wide range of topics, which will facilitate global dialogue and discussion with leading world experts to ceramic technologies for sustainable development of society.

We would like to invite all of you to actively participate in the conference and visit the city of Budapest. We are quite hopeful that this conference will provide excellent forum for interaction and friendship with participants from various continents.

We hope to meet you all in 2024!

About Budapest

Budapest is famous not only for the monuments reflecting its own 1,000-year-old culture, but also for the relics of others who settled here. Remains from both Roman occupation and much later ruled by the Turks can still be seen in the city. After the Ottoman Empire the union with Austria has a particular influence on the city's form and style.

Conference venue

Budapest Congress Center & Novotel Budapest City****Budapest Congress Center is the largest, most convenient, modern event facility in Budapest. It has over 20 meeting rooms in various shapes and sizes, adjustable for every possible need, as well as an exhibition space of over a 4000 m^2, which means it can hold separate events at the same time without them interfering with each other. International congresses, exhibitions, professional conferences, corporate meetings, gala dinners, tradeshows, fairs, concerts, plays or graduation ceremonies – Budapest Congress Center is perfect for them all!

https://akcongress.com/cmcee14

építőanyag
Journal of Silicate Based and Composite Materials
2022/6

TARTALOM

CONTENT

A finomkerámia-, üveg-, cement-, mész-, beton-, tégla- és cserép-, kő- és kavics-, tűzállóanyag-, szigetelőanyag-iparágak szakmai lapja
Scientific journal of ceramics, glass, cement, concrete, clay products, stone and gravel, insulating and fireproof materials and composites

A folyóiratot referálja · The journal is referred by:
ProQuest · Google Scholar · INDEX COPERNICUS INTERNATIONAL · THOMSON REUTERS

A folyóiratban lektorált cikkek jelennek meg.
All published papers are peer-reviewed.
Kiadó · Publisher: Szilikátipari Tudományos Egyesület (SZTE)
Elnök · President: ASZTALOS István
1034 Budapest, Bécsi út 120.
Tel.: +36-1/201-9360 ▪ E-mail: epitoanyag@szte.org.hu
Tördelő szerkesztő · Layout editor: NÉMETH Hajnalka
Címlapfotó · Cover photo: GYURKÓ Zoltán

WWW.EPITOANYAG.ORG.HU
EN.EPITOANYAG.ORG.HU

Online ISSN: 2064-4477
Print ISSN: 0013-970x
INDEX: 2 52 50 ▪ 74 (2022) 207–241

Use of recycled aggregates from different sources in the production of SCC Part I: Mix design and fresh properties

Saad CHAIB
PhD candidate, Department of Civil Engineering, University of Laghouat, Algeria. His research interests include self-compacting concrete, recycled aggregates.

Lakhdar AZZOUZ
Professor at the Department of Civil Engineering, University of Laghouat, Algeria. His research interests include Reuse of local materials, concrete technology.

Benchaa BENABED
Professor at the Department of Civil Engineering, University of Laghouat, Algeria. His research interests include self-compacting concrete, rheology and durability of concrete.

Saad CHAIB ▪ Civil Engineering Research Laboratory (LRGC), University of Laghouat, Algeria
Lakhdar AZZOUZ ▪ Civil Engineering Research Laboratory (LRGC), University of Laghouat, Algeria
Benchaa BENABED ▪ Civil Engineering Research Laboratory (LRGC), University of Laghouat, Algeria
Érkezett: 2022. 03. 03. ▪ Received: 03. 03. 2022. ▪ https://doi.org/10.14382/epitoanyag-jsbcm.2022.30

Abstract
The purpose of this research is to investigate the effect of recycled gravel on the rheological properties of self-compacting concrete (SCC). In this experimental study, five types of gravel were used to prepare nine SCC mixtures with a Water/Binder ratio (W/B) of 0.4 and a binder dosage of 475 kg/m^3. The control SCC is made entirely of regular crushed gravel, whereas the other mixes use recycled gravel to replace the regular crushed gravel to varying degrees. Slump flow by Abrams cone, V-Funnel test, J-Ring test, L-Box test, and sieve stability segregation test were used to investigate the properties of the fresh SCC mixtures. The results show that all SCC mixtures have good deformability and resistance to segregation, with the exception of mixtures made from bituminous mixtures gravel and crushed brick. SCCs of binary mixtures containing two types of gravel (regular crushed gravel and recycled gravel) produce acceptable results that meet the AFGC and EFNARC recommended criteria.
Keywords: recycled concrete aggregates, brick, marble, bituminous aggregates, SCC fresh properties
Kulcsszavak: újrahasznosított beton adalékanyagok, tégla, márvány, bitumenes adalékanyagok, SCC friss tulajdonságai

1. Introduction

The concept of producing fluid concretes that spread in the formwork without the use of vibrating effort is an intriguing solution that allows for uniform structures and the avoidance of possible errors in the placement of the concrete, particularly elements of very complex shape. This is how the concept of self-compacting concrete (SCC) came to be [1]. These very fluid concretes were also very stable and had a high resistance to segregation and bleeding. The technique of concrete poured under water was used to meet the usually contradictory conditions (deformability and resistance to segregation); in fact, the first generation of self-compacting concretes is formulated in the same way as the concretes intended for submerged structures, but with a lower viscosity and thus a higher workability. In order to resist the segregation of large aggregates and the bleeding phenomenon, these concretes frequently contain viscosity agents or colloidal agents. This type of concrete is of particular interest in Algeria, where the imperatives of improved work quality and formwork complexity have become increasingly apparent in recent years. Recycled aggregates are aggregates that have been obtained by recycling concrete from demolition. Indeed, these aggregates have a variety of applications in civil engineering, most notably in road construction and the preparation of concrete for various buildings. Furthermore, current environmental policy encourages their use in order to reduce raw material consumption and comply with environmental regulations. In this context, several studies have been conducted in Algeria and other countries over the last ten years in order to use waste as recycled aggregates in ordinary concrete and SCC. These investigations include the study of the influence of crushed sand by Benabed [2, 3] and the recovery of construction and demolition waste (particularly brick and concrete) by Azzouz et al. [4], Douara [5] and Nezergui [6].

This study focuses on the effect of gravel type characteristics (coarse aggregates) on the properties of SCC in the fresh state. The study aims to evaluate the behavior of SCC based on the physical characteristics of coarse aggregates and the properties of self-compacting mortar in the fresh state. The influence of the type of gravel (ordinary or recycled) and the shape of the gravel grains (flattened or elongated) on the rheological properties of SCC was investigated.

2. Materials and experiments

2.1 Identification and characterization of materials

In this study, Ordinary Portland cement (CEM I 42.5) was used in the preparation of the various SCC mixtures, which were manufactured in accordance to standard NT 47.01 with densities and specific surface areas of 3.15 and 3700 cm^2/g, respectively. The chemical properties of cement and MP are given in *Table 1*. In order to avoid using high cement content and to develop an SCC at a lower cost while also contributing to environmental preservation, a prudent solution consists in using a binary mixture containing the marble powder (MP) as mineral addition [2] with a degree of substitution of 10%, because it gave a fluid and homogeneous mixture. This powder has a density of 2.70 and a fineness of 3600 cm^2/g (*Table 1*). Throughout this study, a single type of third-generation high water-reducing superplasticizer was employed. It is based on polycarboxylates, which significantly improve the fluidity of fresh concrete.

Binder	SiO_2	CaO	MgO	Al_2O_3	Fe_2O_3	SO_3	K_2O	TiO_2	Na_2O	P_2O_5	Loss ignition
Cement	18.83	61.54	1.27	4.20	5.31	1.96	0.49	0.20	0.21	0.29	5.70
MP	0.42	56.01	0.12	0.13	0.06	0.01	0.01	0.01	0.43	0.03	42.78

Table 1 Chemical composition of cement and marble powder MP
1. táblázat A cement és a márvány (MP) kémiai összetétele

1

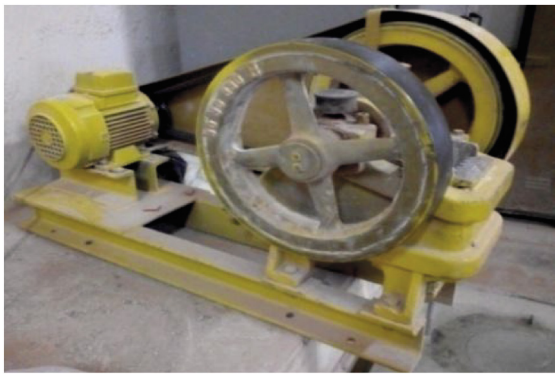

2

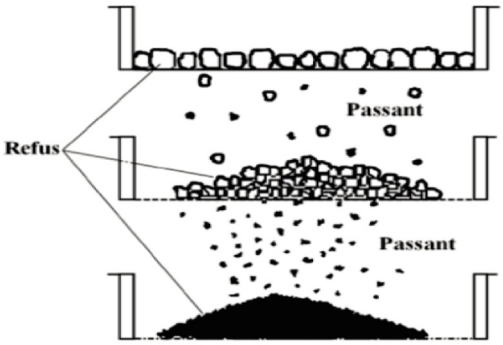

3

Fig. 1 Stages of elaboration and preparation of recycled gravel: 1/- Breaking up the blocks of material used with a hammer. and breaking up the material fragments to dimensions suitable for the opening of the crusher, 2/- Crushing of fragments using a two-jaw crusher, 3/- Screening procedure (separation of the different granular classes 3/8 and 8/16)
1. ábra Az újrahasznosított kavics feldolgozásának és előkészítésének szakaszai: 1/- A felhasznált anyagtömbök törése kalapáccsal és az anyagdarabok aprítása a törőgép nyílására alkalmas méretűre, 2/- A darabok aprítása kétpofás törőgéppel, 3/- Szitálás (a különböző szemcseméretű - 3/8 és 8/16 - frakciók szétválasztása)

Fig. 2 Different types of aggregate used
2. ábra Az alkalmazott aggregátumok

Properties	OCG		WMG		RBG		DCG		BMG	
Size (mm)	(3/8)	(8/16)	(3/8)	(8/16)	(3/8)	(8/16)	(3/8)	(8/16)	(3/8)	(8/16)
Absolute density	2.691	2.673	2.71	2.695	2.216	2.227	2.568	2.592	2.286	2.292
Apparent density	1.365	1.395	1.368	1.392	0.946	0.949	1.127	1.18	1.128	1.048
Compactness (%)	50.72	52.19	50.48	51.65	42.69	42.61	43.89	45.52	49.34	45.72
Porosity (%)	49.28	47.81	49.52	48.35	57.31	57.39	56.11	54.48	50.66	54.28
Water absorption (%)	2.31	1.46	0.44	0.28	10.91	9.67	8.23	5.90	1.11	1.60
Surface cleanliness (%)	0.29	0.19	0.81	0.18	0.78	0.26	1.79	1.27	0.28	0.39
Elongation coefficient	0.33	0.57	0.30	0.48	0.34	0.37	0.39	0.64	0.42	0.62
Kurtosis coefficient	0.33	0.45	0.38	0.39	0.33	0.48	0.33	0.43	0.33	0.47
Los-Angeles (%)	25.1	21.1	32.7	28.3	42.8	46.3	34.5	26.4	23.8	25.6
Micro-Deval (%)	8.2	5.2	8.1	15.6	16.1	36.8	12.9	11.2	8.4	11.9

Table 2 Properties of the aggregates used
2. táblázat A felhasznált adalékanyagok tulajdonságai

A river sand SA (0/5) of siliceous nature was used with density of 2.65 for the preparation of SCC mixes. An ordinary crushed gravel (OCG) of limestone nature, and four types of recycled gravel produced in the laboratory *(Fig. 1);* recycled gravel (WMG) made from crushed white marble waste, recycled gravel (RBG) made from crushed red brick waste, recycled gravel (DCG) made from crushed demolition concrete, and recycled gravel (BMG) made from milling and recycling bituminous mixtures. They are divided into two granular classes of each type (3/8 and 8/16) as shown in *Fig. 2*. The different properties of the aggregates used are summarized in *Table 2*. The particle size analysis was performed in accordance with standard NF EN 933-1 [7], and the particle size curves of the various aggregates are shown in *Fig. 3*.

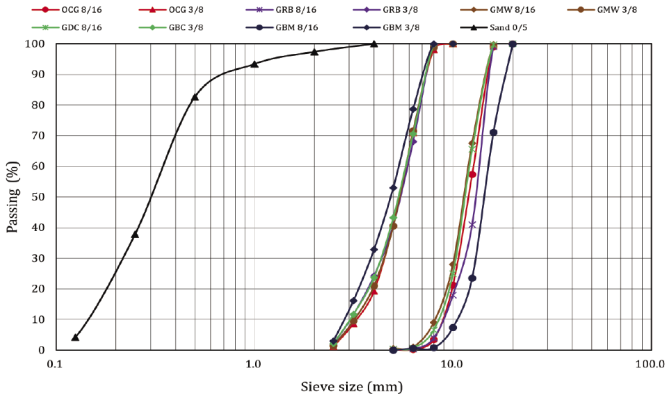

Fig. 3 Particle size curves of the different aggregates studied
3. ábra A vizsgált aggregátumok szemcseméreteloszlása

2.2 Mix-design of SCC

The self-compacting mortar (SCM) phase is critical in the mix-design of SCC, because it provides lubrication between the coarse aggregate particles, viscosity, mobility and overall SCC stability. SCM's properties are similar to those of SCC, namely a low shear threshold to ensure flow under gravity alone and sufficient plastic viscosity to ensure non-segregation concrete during flow. Simpler alternative tests for assessing the fluidity of SCM are proposed, such as the mini-slump test and the mini-funnel test (V-funnel) [8]. The Okamura method was used to formulate the SCM, with improvements in the sand content (S/M) and the water/binder ratio (W/B). The slump test, in which the diameter (D) obtained must be between (270 mm D 330) [9], and the V-funnel test, in which the flow time obtained must be between 2-10 s [8], are used to adjust the superplasticizer/binder ratio (Sp/B).

According to Jin and Domone [8], mortar tests are performed because SCC has a smaller bulk aggregate volume than ordinary concrete and thus the mortar's properties are dominant. Because the evaluation of the properties of the mortar is an integral part of the formulation of the SCC, knowing of the properties of the mortar is useful. As a result, testing mortar is far more convenient and straightforward than testing concrete (*Fig. 4*).

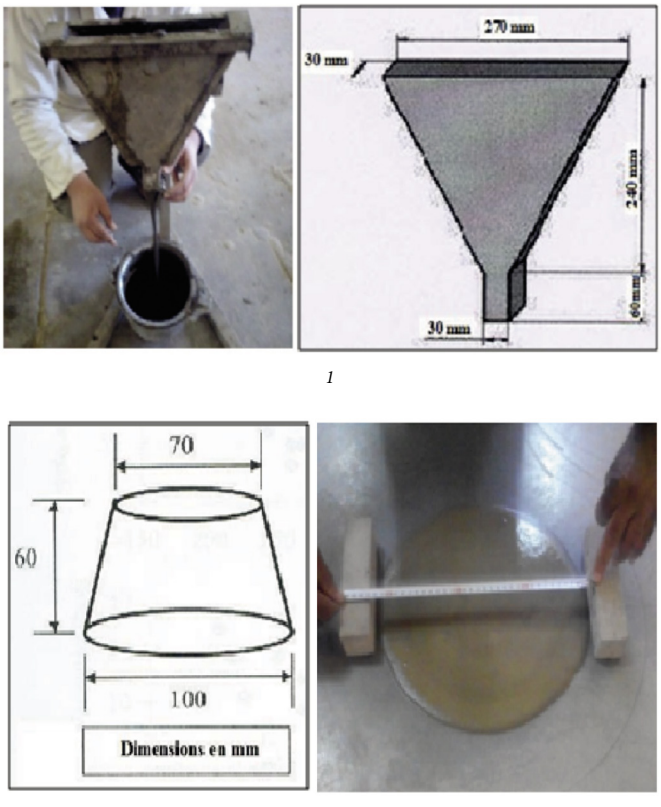

Fig. 4 Self-compacting mortar (SCM) tests: 1/ Mini slump cone test 2/ Mini V-funnel
4. ábra Öntömörödő habarcs (SCM) vizsgálatok

S/M = 0.5 W/B = 0.4 Constituents		Family A					Family B			
		SCC 1 100% OCG	SCC 2 100% WMG	SCC 3 100% BMG	SCC 4 100% DCG	SCC 5 100% RBG	SCC6 (50%OCG +50%WMG)	SCC7 (50%OCG +50%BMG)	SCC8 (50%OCG +50%DCG)	SCC9 (50%OCG +50%RBG)
Cement (kg/m³)		433.7	433.7	433.7	433.7	433.7	433.7	433.7	433.7	433.7
Marble powder (kg/m³)		41.3	41.3	41.3	41.3	41.3	41.3	41.3	41.3	41.3
Sand (kg/m³)		901.5	872.3	916.6	937.7	960.5	883.1	901.9	914.7	920.7
Ordinary gravel (kg/m³)	(8/16)	546.0	—	—	—	—	281.7	246.9	254.6	231.8
	(3/8)	270.8	—	—	—	—	139.6	122.4	126.2	114.9
Recycled gravel (kg/m³)	(8/16)	—	588.3	444	451.9	350.2	285.0	247.8	243.2	212.5
	(3/8)	—	293.7	220.9	221	172.7	142.3	123.3	118.9	104.8
Water (kg/m³)		197.0	182.9	205.6	252.8	273	193.0	202.7	228.4	240.3
Superplasticizer	Sp (%)	1.00	1	1	0.9	0.9	1	1	1	1
	Sp (kg/m³)	4.8	4.8	4.8	4.3	4.3	4.8	4.8	4.8	4.8

Table 3 Mix-proportions of the different SCC
3. táblázat Az öntömörödő betonok (SCC-k) keverékarányai

The results of slump and flow time tests on SCC enabled the following conclusions to be drawn:

- The slumps and flow times obtained are between 303 mm and 324 mm and 2.69 and 3.46 s, respectively, and are consistent with the values proposed by Domone and Jin [8].
- The ratios S/M = 0.5 and W/B = 0.4 will be used for all mortars in the following work because they produce fluid and homogeneous mortars.
- Sp/B ratio = 1.0% will be used in the rest of the work because it produced a fluid and homogeneous mixture that met the three SCM criteria.
- MP with content of 10% will be used in the following work for all SCC mixtures because it produces fluid and homogeneous mortars.

In the laboratory, nine different SCC mixtures were prepared. These mixtures contain coarse aggregates with a maximum diameter of 16 mm, and recycled gravel was used as a replacement for ordinary gravel at substitution rates by volume of 0, 50, and 100%. All of the compositions have a powder content of 475 kg/m³, W/B ratio of 0.4 and S/M ratio of 0.5. Mix-proportions of the different types of SCC are given in *Table 3*.

3. Experimental results

3.1 Slump flow test

3.1.1 Slump

According to EFNARC [10], a concrete with a diameter of 650-800 mm in the slump flow test is considered a BAP. According to *Fig. 5*, it should be noted that all SCC mixtures have slump values between 682-765 mm, which falls within the previously mentioned range. As a result, most of mixtures are within the range of BAP class SF2 (660 to 750 mm) according to AFGC [11], with the exception of the BAP3 mixture (based on BMG), which is within the range of class SF3 (760 to 850 mm). As a result of the AFGC [11] recommendations, all SCC mixtures are characterized by good deformability. SCC5 made with crushed brick gravel (RBG) has a minimum slump of 682 mm. This is because coarse aggregates have a flat and elongated shape. The latter absorb more water and thus have a higher demand for it. As a result, the workability of the concrete is reduced. Aarre and Domone [12] recommend a slump of 650 mm to 700 mm for good SCC.

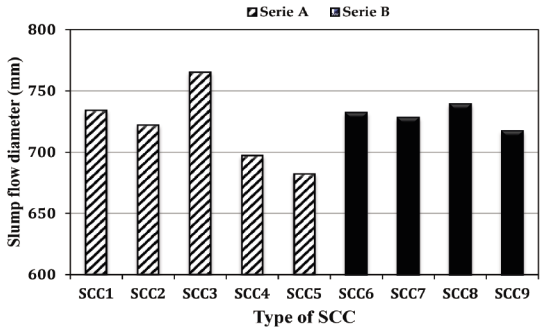

Fig. 5 Slump flow results of the different types of SCC
5. ábra Az öntömörödő betonok (SCC-k) zsugorodási eredményei

3.1.2 Slump flow time T500

The time required to reach a diameter of 50 cm is the second parameter entered into the Abrams cone slump test. *Fig. 6* depicts the results of the flow time T500. It should be noted that, the flow time T500 results of all SCC are lower than those proposed by Domone et al. [9]. This is most likely explained by the mixtures' high viscosity. The lowest flow time is found in the mixture of SCC3 of family A made with gravel of bituminous mixtures (GBM), as shown in *Fig. 6*, and this can be justified by its large high slump (765 mm) and the value of the minimum T500 equal to 0.95 s.

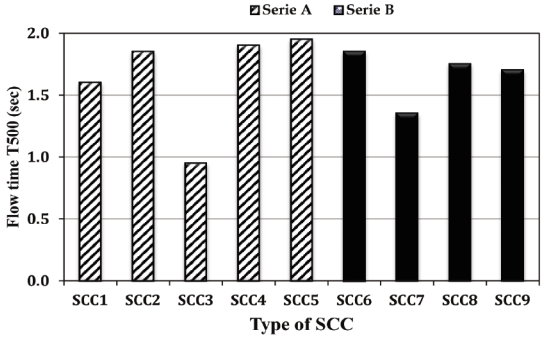

Fig. 6 T500 results of the different types SCC
6. ábra A különböző típusú öntömörödő betonok (SCC-k) T500 eredményei

3.2 J-ring test

The J-ring test is simple to perform and provides an accurate measurement of workability loss in the presence of obstacles. Daczko [13] suggests comparing slump measurements without and with the J-ring present for this purpose.

3.2.1 J-ring slump flow (SJ)

Fig. 7 depicts histograms of the J-ring slump results. It can be seen the clear difference in the slump values of the mixtures when the J-ring is absent versus present for all of the mixtures with the same rate. This distinction is interpreted by the blocking caused by the J-obstacles ring. It is also observed the increase in the slump of the J-ring of SCC3 of family A made with recycled gravel (BMG), which has a significant value and provides the best value (728 mm). In comparison to SCC4 and SCC5 (100% recycled gravel) mixtures of the family A, SCC8 and SCC9 of the family B (50% OCG + 50% recycled gravel) exhibit a large slump of J-Ring.

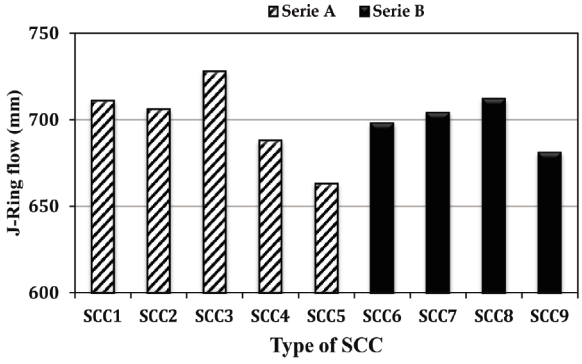

Fig. 7 J-Ring flow results of the different types of SCC
7. ábra J-gyűrűs áramlási eredmények a különböző öntömörödő betonoknál (SCC)

Table 4 shows the flow of SCC as a function of the flow difference without and with J-ring [14]. Based on these findings, it is possible to conclude that, the mixtures (SCC1, SCC2, SCC4, SCC5, and SCC7) have an adequate passage capacity and resistance to segregation in heavily reinforced areas.

Mix.	Slump – Slump (J-Ring) (mm)		Evaluation of flow
SCC1 (100%OCG)	23	(0 - 25)	Good flow
SCC2 (100%WMG)	16		
SCC4 (100%DCG)	9		
SCC5 (100%RBG)	19		
SCC7 (50%OCG+50%BMG)	24		
SCC3 (100%BMG)	37	(> 25 - 50)	Partially blocked flow
SCC6 (50%OCG+50% WMG)	34		
SCC8 (50%OCG+50%DCG)	27		
SCC9 (50%OCG+50%RBG)	36		

Table 4 Flow of different types of SCC according to the difference in slump without and with the ring
4. táblázat A különböző típusú öntömörödő betonok (SCC-k) folyása a gyűrű nélküli és a gyűrűvel való süllyedés különbsége alapján

3.2.2 J-ring slump flow time T500J

The J-ring test determines the capacity of passage to fill all voids. The flow time T500J results for the various SCC mixtures are translated into histograms in *Fig. 8*. The flow time T500 (1.25 s–2.40 s) in the presence of the J-Ring is acceptable when compared to the absence of the J-Ring for all types of SCC. As a result, the SCC passage capacity is suitable for all compositions. The delay is significant for SCC2 mixtures made with marble waste gravel (WMG) and SCC5 mixtures made with crushed brick gravel (RBG). This is because gravel grains are flat and elongated.

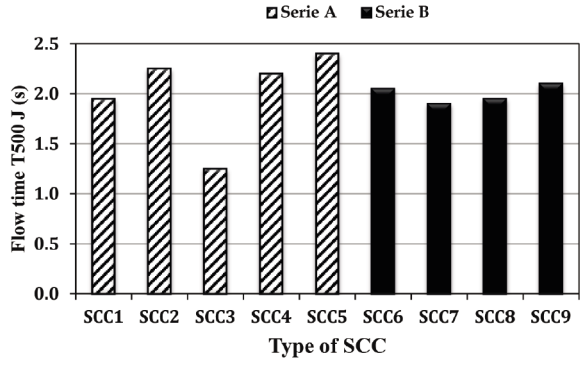

Fig. 8 T500 J-Ring result of the different types of SCC
8. ábra Az öntömörödő betonok (SCC) T500 J-gyűrű eredményei

3.2.3 Height of J-ring slump flow (Difference in height: Bj)

It is widely accepted that in order to mitigate the risk of non-blocking, the difference in height (Bj = Hint – Hext) must be less than 20 mm. According to some authors [15], the risk of non-blocking is only satisfied if Hint - Hext ≤ 15 mm. *Fig. 9* depicts the height of flow (Bj) results obtained from J-ring tests. It should be noted that the risk of mixtures blocking is low for the majority of the mixtures. SCC5 and SCC9 mixtures containing flat and elongated gravel grains, but low for SCC2.

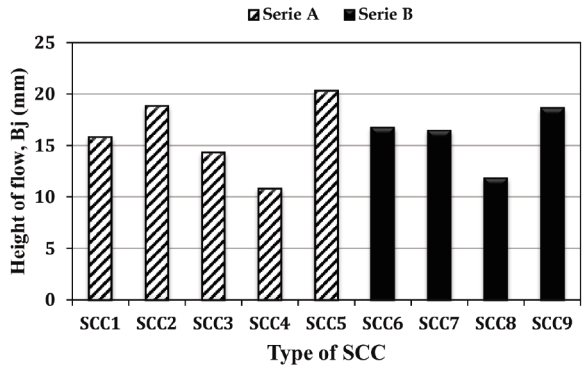

Fig. 9 Difference in height BJ-Ring of the different types of SCC
9. ábra Az öntömörödő betonok (SCC) BJ-gyűrű magasságkülönbségei

3.3 V-funnel flow time test

One method for determining the viscosity and resistance to segregation of SCC is to test the flow through the V-funnel. According to Domone and Jin [8], the flow time values range between 2-10 s. Based on the obtained results, it can be concluded that, all SCC mixtures produce good results with flow time ranging between 5.3-7.35 s. SCC3 of family A made from bituminous mixtures gravel yields the lowest flow time value (BMG).

Sonebi and Bartos [16] achieved a T500 time of less than 2 seconds with SCC mixture containing approximately 40% more paste than ordinary concrete. SCC4 of family A achieves the highest value (7.35 s) using crushed concrete gravel (GDC). This is explained by an increase in the mixture's compactness, and thus an increase in viscosity [17].

Safawi et al. [18] demonstrated that the V-Funnel flow time is an appropriate tool for describing the tendency of segregation. As a result, the tendency for concrete to segregate is very high for very short flow times (less than 2 s). This implies that low viscosity mixtures segregate easily. If there is too much aggregate, for example, the inverted cone shape will obstruct the flow of concrete. On the other hand, a high flow time can be associated with low deformability due to high paste viscosity and/or high intergranular friction [19]. SCC4 and SCC5 mixtures have a higher viscosity than the others, resulting in V-funnel blocking. This is due to type of gravel's, grain water consumption as well as the grain settling effect.

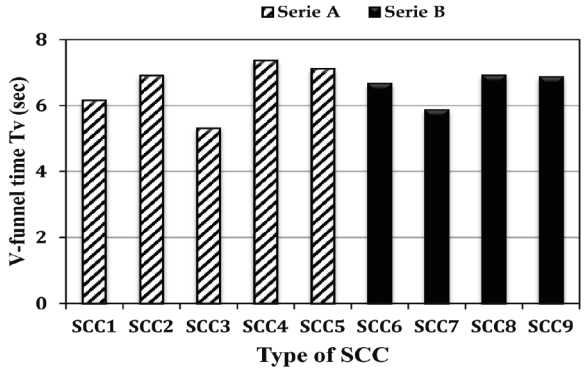

Fig. 10 Flow time results of the different types of SCC
10. ábra Az öntömörödő betonok (SCC-k) folyási idő eredményei

3.4 Sieve stability segregation test

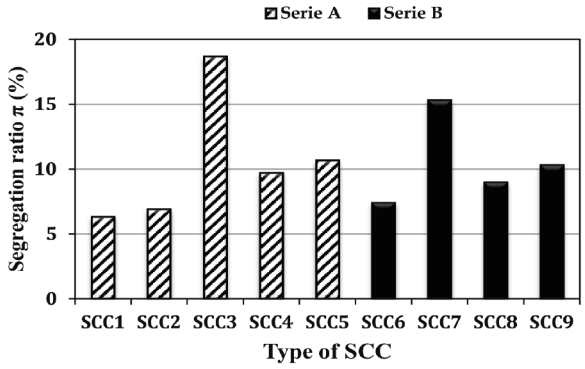

Fig. 11 Resistance to segregation π (%) of the different types of SCC
11. ábra Az öntömörödő betonok (SCC-k) π szegregációval szembeni ellenállása (%)

According to AFGC recommendations [11], the optimum percentages of cement grout passing through the sieve are between 0% and 15%. By using recommended values, it is clear that, the majority of SCC mixtures have good resistance to segregation and bleeding, except for mixtures of bituminous mixtures gravel SCC3 (100% BMG) and SCC7 (50% BMG), which have higher percentages (>15%) than other SCC mixtures due to low viscosity. As a result, these SCC are less viscous and unstable. On the one hand, the large amount of mortar (sand + cement) contained in SCC, the nature of the addition and the type of gravel used, ensure good resistance to segregation. According to Corinaldesi and Moriconi [20], mixtures of SCC with 100% crushed concrete gravel and stone powder as mineral additions may have improved flowability and segregation resistance.

3.5 L-Box test

The L-Box test is notable for providing an accurate assessment of three capacities: filling, passage, and resistance to segregation. *Fig. 12* depicts the results of varying the H_2/H_1 ratio based on the type of gravel. The gravel substitution had no effect on the SCCs' filling capacity. The H_2/H_1 ratio varies between 80.42% and 93.7% for all SCC (except SCC5). As a result, this ratio exceeds 80% as required by EFNARC recommendations [10].

The H_2/H_1 ratio of SCC5 made from gravel (RBG) remains below the EFNARC limit. This may be explained by the flattened and elongated shape of the coarse aggregates. This latter causes a decrease in the H_2/H_1 ratio and increases the risk of gravel blocking behind the steel bars of the L-Box [21]. The results show that when ordinary crushed gravel (OCG) is completely or partially replaced by crushed concrete gravel (DCG), the L-box filling capacity improves for the SCC4 and SCC8 mixtures.

Three parameters influence the H_2/H_1 ratio, according to Sonebi et al. [21]: the amount of water, the amount of coarse aggregates in the mixture and the amount of superplasticizer. The first two parameters increase the H_2/H_1 ratio but increasing the dosage of aggregates decreases the H_2/H_1 ratio and increases the risk of blocking of the coarse aggregates behind the steel bars of the L-Box.

3.6 Visual examination of SCC static segregation

The vertical (static) segregation control test of SCC mixtures is a very simple test and consists of sawing the hardened concrete specimen in the direction of the pour and directly observing the aggregate distribution over the height of the concrete. *Fig. 13* clearly shows that the nine SCC mixtures presented here are not subjected to static segregation. In fact, the aggregates are evenly distributed across the entire height of the sawn samples. This observation was made in all cases and resulted in the same conclusion.

The results demonstrated that limiting sieve stability to 15% is slightly severe, as concretes with sieve values greater than 15% (SCC3 and SCC7) did not exhibit static segregation. The L-box test simulates concrete flow in reinforced formwork. This test allows you to determine whether or not there is concrete blockage at the reinforcing bar level. The sieve stability test results can be used to make a judgment about vertical segregation.

Vertical segregation is not a significant risk in an SCC with a viscous and cohesive paste. However, this method remains an indirect appreciation of static segregation. Given the high fluidity of SCC, the risk of vertical (static) segregation is not insignificant. As a result, it is critical to inspect the uniformity of the granular skeleton in the concrete mass. Bensebti et al. [22] demonstrated that this type of segregation is not visible and can only be observed using very advanced techniques.

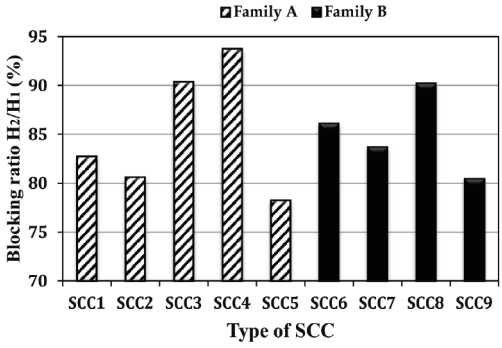

Fig. 12 L-Box test results of the different types of SCC
12. ábra Az öntömörödő betonok (SCC-k) L-Box vizsgálati eredményei

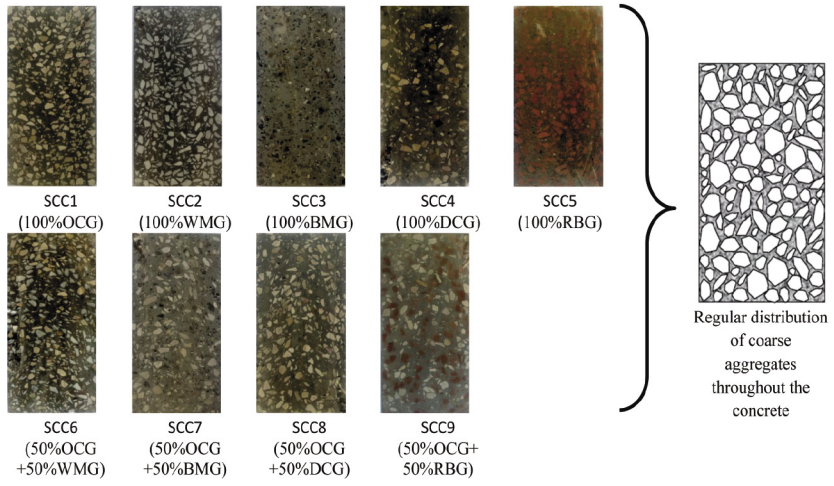

Fig. 13 Visual examination of static segregation of the different types of SCC
13 ábra Az öntömörödő betonok statikus szegregációjának vizuális vizsgálata

4. Conclusions

Based on the findings of this study, a number of conclusions can be made including the following:

- Ordinary crushed gravel (OCG) SCC is found to meet the wet state properties required by EFNARC and AFGC recommendations;
- Crushed marble waste gravel (WMG) has fairly similar wet characteristics, but use of this type of gravel (WMG) is ineffective, because it is very expensive;
- Crushed brick gravel (RBG) significantly reduces SCC slump, due to the flat and elongated shape of gravel (RBG) as well as the high water absorption.
- Incorporating of Bituminous mixtures (BMG) in SCC appears to improve deformability but exhibits poor resistance to segregation and bleeding.
- The risk of mix blockage is low for most SCC mixes, but high for mixtures of marble waste gravel (WMG) and crushed brick gravel (RBG) containing coarse aggregate grains of flat and elongated shape.
- The minimum value of the V-funnel flow time is obtained for SCC3 made from bituminous gravel (BMG). SCC4 crushed concrete gravel (DCG) and SCC5 crushed brick gravel (RBG) mixtures have higher viscosity than the other mixtures, resulting in V-funnel blocking. This is due to each type of gravel's grain water consumption as well as the grain settling effect.
- To improve SCC's static stability and resistance to segregation, the coarse aggregate content is reduced while the fines content is increased.

Acknowledgements

The authors gratefully acknowledge the Directorate-General of Scientific Research and Technological Development of Algeria (DGRSDT) for its valuable support.

References

[1] Okamura. H., Ozawa K. "Self-compac high performance concrete in Japan" ACI International Workshop on high Performance Concrete. Bangkok. Thailand. 1994.

[2] Boukhelkhal A., Azzouz L., Belaïdi A., Benabed B. "Effects of marble powder as a partial replacement of cement on some engineering properties of self-compacting concrete" Journal of Adhesion Science and Technology. 2016. Vol. 30. No. 22. pp. 2405–2419. https://doi.org/10.1080/01694243.2016.1184402

[3] Benabed B. "Influence of sand type on performance and durability of SCC" PhD Thesis. University of Laghouat. 2014

[4] Azzouz L., Bouhicha M., Kenai S. "Valorisation and recycling of brick wastes in sand concrete" Magazine of Laghouat University. Vol.3. N°1. Mai.2001.

[5] Douara T-H. "Influence of additions on the quality of concrete based recycled aggregates" Msc thesis. ENSET Oran. 2008

[6] Nezergui B. "Comparative study on the formulation of SCC based recycled and ordinary aggregates" Msc thesis. ENSET Oran. 2008.

[7] NF EN 933-1. "Aggregates tests - Part 1: particle size analysis of aggregates" (1997) AFNOR.

[8] Domone P.L. Jin J. "Properties of Mortar for Self-Compacting Concrete dz. Proceedings of the 1st International Symposium on Self-Compacting Concrete" RILEM Proceedings (PRO 7). Edited by Å. Skarendahl and Ö. Petersson Stockholm. Sweden. 1999. pp. 109 – 120.

[9] Domone. P.L., Chai. H.W. Jin J. "Optimum mix proportioning of self-compacting concrete. Proceeding on international conference on innovation in concrete structures: design and construction" University of Dundee. ed Dhir RK and Jones MR. Thomas Telford. London.

[10] EFNARC. "Specifications and Guidelines for Self-compacting Concrete" European Federation of Producers and Applicators of Specialist Products for Structures. EFNARC. Norfolk. UK. February 2002. p. 32.

[11] Association Française de Génie Civil. "Bétons auto-plaçants - Recommandations provisoires" Annales du bâtiment et des travaux publics. 2000.

[12] Aarre T., Domone P. "Reference concretes for evaluation of test methods for SCC" Proceedings of 3rd RILEM International Symposium on Self Compacting Concrete. Reykjavik. Iceland. 2003. pp. 495-505.

[13] Daczko J.A. "A comparison of passing ability test methods for Self-Compacting Concrete" 3rd International Symposium on Self Compacting Concrete. 17-20 August 2003. Reykjavik. Iceland. pp. 335-344.

[14] ASTM C 1621. "Standard Test Method for Passing Ability of Self-Compacting Concrete by J-Ring" American Society for Testing and Materials. USA. 2009.

[15] Wüstholz T. "A model approach to describe the fresh properties of self-compacting concrete (SCC)" Otto-Graf Journal. 16. 2005.

[16] Sonebi M., Bartos P.J.M. "Hardened SCC and its bond with reinforcement" Proceeding of First International RILEM Symposium on Self-Compacting Concrete. Stockholm. Sweden. 1999. pp. 275-289.

[17] Gritsada S.I., Natt M. "Utilization of limestone powder to improve the properties of self-compacting concrete incorporating high volumes of

untreated rice husk ash as fine aggregate" Construction and Building Materials 38. 2013. pp. 455 – 464. https://doi.org/10.1016/j.conbuildmat.2012.08.016

[18] Safawi M.I., Iwaki I., Miura T. "A study on the applicability of vibration in fresh high fluidity concrete" Cement and Concrete Research. 2005. vol 35. pp. 1834–1845. https://doi.org/10.1016/j.cemconres.2004.10.031

[19] R'mili A. "Formulation and behavior of SCC: Incorporation of crushed sand and desert sand" PhD thesis. 2010. p. 238

[20] Corinaldesi V., Moriconi G. "The role of industrial by-products in self-compacting concrete" Construction and Building Materials dz. 2011. Vol. 25. pp. 3181-3186. https://doi.org/10.1016/j.conbuildmat.2011.03.001

[21] Sonebi M., Grünewald S., Walraven J. "Filling ability and passing ability of Self-Compacting Concrete" ACI Materials Journal. March/April 2007. pp. 162-170.

[22] Bensebti S., Chabane A., Aggoun S., Houari H. "Vertical segregation of SCC; Setting up an experimental procedure" Rencontres Universitaires de Génie Civil. May 2015. Bayonne. France.

Ref.:
Chaib, Saad - **Azzouz**, Lakhdar - **Benabed**, Benchaa: *Use of recycled aggregates from different sources in the production of SCC. Part I: Mix design and fresh properties*
Építőanyag – Journal of Silicate Based and Composite Materials, Vol. 74, No. 6 (2022), 210–217. p.
https://doi.org/10.14382/epitoanyag-jsbcm.2022.30

Corrosion behaviour and surface topography for steel plates used in automotive industry exposed to salty corrosive thermo-accelerated medium

Shaymaa Abbas ABDULSADA
PhD in Metallurgy, Materials Department, Faculty of Engineering, University of Kufa, Iraq. Research Interests: Materials Testing and Processing, Engineering of Metallurgy, Corrosion Engineering, Heat Treatment of Metals, Casting of Metals, Non-Metals Degradation.

Ali I. AL-MOSAWI
PhD in polymers Engineering at Institute of Ceramic and Polymer Engineering, Faculty of Materials Science and Engineering, University of Miskolc, Hungary. Research Interests: Polymers, Composite Materials, Rubber Technology, Flame Retardants, Materials Testing, Materials Processing.

Shaymaa Abbas ABDULSADA ▪ Faculty of Engineering, University of Kufa, Iraq
Ali I. AL-MOSAWI ▪ Institute of Ceramic and Polymer Engineering, University of Miskolc, Hungary ▪ alialmosawi76@gmail.com

Érkezett: 2022. 06. 14. ▪ Received: 14. 06. 2022. ▪ https://doi.org/10.14382/epitoanyag-jsbcm.2022.31

Abstract
Corrosion resistance is one of the essential criteria in the automotive industry, especially in harsh climates, as it causes severe damage to vehicles. Therefore, the anti-corrosion factor should be a complementary and integral part of other safety standards. An experimental investigation for monitoring and evaluating the corrosion behavior of high strength low carbon steel plates with different surface characteristics and treatments conditions used in the automotive industry exposed to a salty, corrosive thermo-accelerated medium has been introduced in this empirical study. The produced samples are divided into four main groups: welded, unwelded, coated, and uncoated. These samples were exposed to an aggressive chemical medium consisting of salty-aqueous spray with a 5% NaCl concentration at 35 °C with speed and pressure. All changes in surface features, including topography, roughness, and corrosion products, were measured and analyzed periodically every 8 hours for 24 hours by scanning electron microscopy, optical microscopy, and CSPM imager surface roughness analysis. The results showed that the coated samples had lower roughness values and lower corrosion products after 24 hours under the salty-aqueous spray test.
Keywords: Automotive corrosion, Salty corrosive medium, Zinc coating, Roughness
Kulcsszavak: Autóipari korrózió, sós korróziós közeg, cinkbevonat, érdesség

1. Introduction

Since the 1930s, rock salt has started to be sprayed on roads in the winter to de-ice and prevention of the formation. Adding salt (or salty solutions) reduces the freezing point of water to below -20°C, where the salt acts as an inhibitor of the ability of water molecules to form solid ice crystals so they remain liquid [1, 2]. Although this method saves thousands of lives and prevents thousands of accidents annually, on the other hand, it has caused pollution and the emergence of many of its adverse effects on plants, insects, aquatic animals, water sources, and wetlands, close to these roads [3-9]. Furthermore, a significant problem has been arisen for cars due to salt spray which is corrosion. Repeated exposure to salt affects the unpainted parts of the car and the painted parts. As the coating layer becomes unstable and micro-holes begin to appear, which allows the penetration of water and its contents of salts, leading to the formation of underneath bubbling up. Eventually, the coating layer begins to flake off. Rusty metal layers appear under it, which will soon flake off and fall, resulting in the holes if not treated [10-14]. Therefore, it is essential to consider the issue of corrosion in vehicles at a level not less than other safety factors such as body stiffness, strength, airbags, crash severity sensing, fuel consumption efficiency, fire resistance, and so on [15-17].

A wide range of metals and alloys are used in the automotive industry, including, steels, aluminium alloys, composite materials, and other lightweight materials, So, according to this diversity, the corrosion behavior varies from one material to another of these materials. Many types of steels are used in the automotive industry, the most common being high-strength steel, with various grades, and mild steel, as shown in the *Fig. 1*, represents the safety cage of Volvo XC60 which indicates the materials used in its manufacture [18-28]. The use of a high-strength steel in the vehicle's body can be increased the capacity for energy absorption and plastic deformation resistance of the component. To maintain weldability and formability of automotive parts, high-strength steel will have a low alloying and carbon content, with several alloying elements such as titanium, copper, vanadium, and niobium, which are added to obtain a strengthened structure [29-33]. Electrochemical reactions mainly cause corrosion in automobiles, in addition to other corrosives such as humidity, temperature, a range of air contaminants like chlorine, sulphur oxides, nitrogen oxides, de-icing salts that are the subject of this study. The steel is immersed in a suitable electrolyte, such as water or road salt, and certain localized anodes and cathodes are created. Electrons move from the anodes to the cathodes during anodic oxidation and cathodic reduction, as seen in *Fig. 2* [34-37]. There are many techniques used for corrosion protection and the most common of which is zinc coating or as it is called galvanization. Coating by Zinc provides good corrosion resistance to steel through cathodic control. The zinc coating layer has an effective adhesion to the steel surface which will improve the corrosion and abrasion resistance due to the characteristics of the galvanizing process. Besides the effectiveness of this technology, it is also considered as low cost and easier to implement compared to other technologies [36, 38-41].

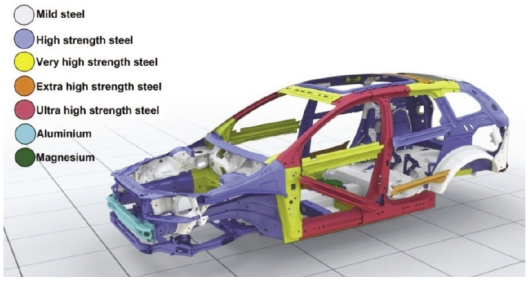

Fig. 1 Materials of Volvo XC60 safety cage [18]
1. ábra A Volvo XC60 biztonságiváz anyagai [18]

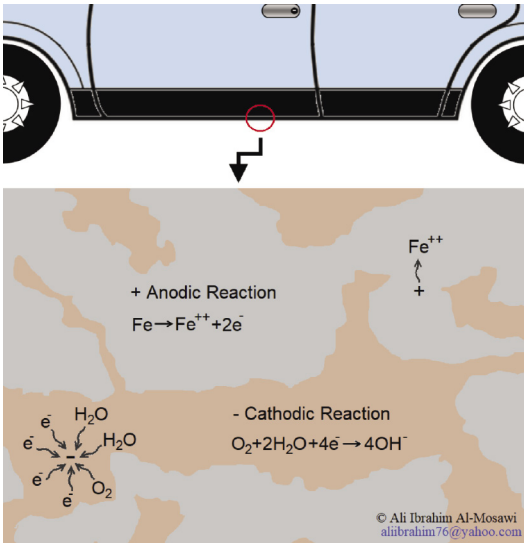

Fig. 2 Corrosion of an automotive body structure
2. ábra Az autóipari karosszéria szerkezetének korróziója

2. Materials and methods

2.1 Materials used

High strength low alloy steel was used in this study. The chemical composition analysis of high-strength low carbon steel shown in *Table 1* was carried out by the ICP-OES method using spectrometer 720 ES.

Chemical composition, %									
C	S	Mn	Si	P	Cr	Ni	Cu	Mo	V
0.07	0.012	0.230	0.140	0.010	0.022	0.036	0.050	0.002	0.003

Table 1 Chemical composition of high strength low alloy steel
1. táblázat Nagy szilárdságú, alacsony ötvözetű acél kémiai összetétele

2.2. Samples preparation

Four samples of high strength low alloy steel (HSLA) plates with dimensions of 5 cm width, 5 cm length, and 1 mm thickness, whose details are illustrated in *Table 2*, were used in this study. The welding process is done using tungsten inert gas arc welding (TIG welding) by Elektra Beckum Industrie WIG 160 DCI. Stress relieving heat treatment was performed at 120 °C for 1 hour, after the cutting and welding process. To provide the optimum surface adhesion, the samples have been cleaned by immersion for 1 min in a dilute HCl mixed with 2 ml of hexamethylenediamine (HMD) corrosion inhibitor to mitigate the effect of HCl on the sample surface upon immersion. After removing the samples from the cleaning solution, they are washed with distilled water, then dried with cotton and placed in a closed container containing a moisture barrier to prevent their oxidation. All sides of the samples are completely coated with a layer of a 200 µm thickness of liquid zinc spray type MAESTRO. The thickness of the coating layer was measured by paint thickness tester PCE-CT 25FN. A summary of the processing steps shown in *Fig. 3*.

Sample	Treatment condition
1	Unwelded and uncoated
2	Unwelded and coated
3	Welded and uncoated
4	Welded and coated

Table 2 Details of test samples
2. táblázat Vizsgálati minták részletezése

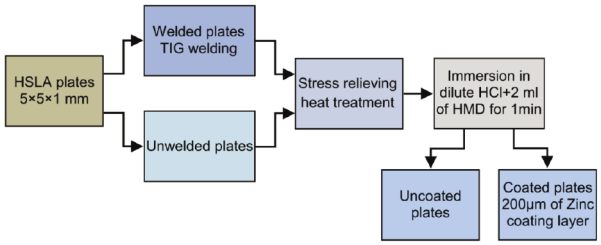

Fig. 3 Processing steps of HSLA plates
3. ábra A HSLA lemezek feldolgozási lépései

2.3 Tests

2.3.1 Salt spray

Thermo-accelerated salt spray test under 5% NaCl salt spray was used to simulate corrosion conditions in natural atmospheres was done according to ISO 9227 [42]. Salt spray cabinet model SF/450 found at University of Miskolc, Hungary was used to complete this test. All surface characteristics of the samples have been recorded before the test started. All surface changes were measured and analyzed during three specific periods, 8, 16, and 24 hours, respectively at 35°C.

2.3.2 Scanning Electron Microscopy (SEM)

This analysis used to determine the spatial distribution of corrosion products on the surface of samples by Carl Zeiss EVO MA10 SEM found at the University of Miskolc in Hungary.

2.3.3 Optical Microscopy

In this surface inspection, Carl Zeiss light optical microscopy with a magnification of 50x was used to detect the extent and spatial distribution of rust, and secondary precipitated phases at the surface of the samples.

2.3.4 Surface roughness

The CSPM imager program shown in *Fig. 4* has been used to surface roughness mapping and evaluation parameters. The investigated surface roughness parameters were mainly the average of the roughness profile (Sa) and core roughness depth (Sk). This superficial evaluation was done according to ISO 21920 for profiles [43, 44] and ISO 25178 for 3D measurements [45].

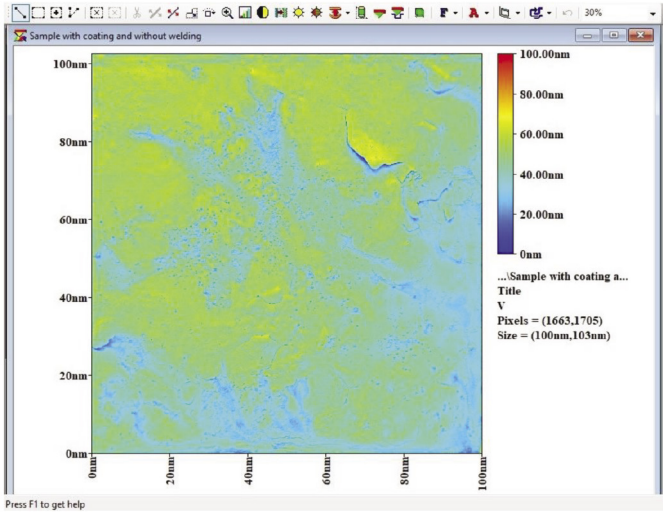

Fig. 4 The CSPM imager program
4. ábra A CSPM imager program

3.Results and Disscusion

3.1 SEM analyses for Surface corrosion products

In such an artificial environment with precipitating salty water with 5% NaCl that mimic the natural conditions of corrosion, HSLA steel plates start corroding in the aqueous salt solution containing dissolved oxygen according to electrochemical reaction mechanism, therefore, there will be migrating tiny local anode and cathode sites with iron dissolution (which will oxidized to ions) and oxygen reduction, respectively. Then the iron(II) and iron(III) cations can react with the anions (first of all OH- anions) present nearby with the formation of soluble and non-soluble oxide-hydroxides and other corrosion products depending on the actual local electrochemical reactions and physical transport circum- stances (diffusion, the solution flows, etc.) [46]. Surface inspection of the samples after exposure to 5% NaCl salt spray for 24 hours has been accomplished by SEM-EDX analysis, and the details are shown in *Fig. 5* and *Fig. 6*, respectively. The corrosion products of this process are listed as oxides in *Table 3*. In *Fig. 5*, the unwelded and uncoated sample showed a severe oxidized surface state that extended over most of the surface, and this state is very clear in *Fig. 6* as well. The chemical composition of this oxidized surface contained about 86.53 wt.% FeO. The analysis also showed that the surface of the unwelded and uncoated sample contained some compound-bound chlorine (Cl_2O) with a quantity of 10.55 wt.%. This indicates that the chloride ions migrated or penetrated the steel surface. Since the chloride ions can quickly and easily dissipates because this sample does not have any protective layer. These ions will initiate and/or develop their corrosion layer through the possible subsequent formation of various iron-oxide-hydroxide (rust) compounds.

In the unwelded and coated sample, the oxidized surface state was reduced by 94.5%, where the FeO content has been decreased from 86.53 wt.% to only 4.75 wt.%. The FeO formation on the coated sample surface is because of the possibility of creating microcracks in the areas of invisible defects of the zinc coating layer resulting from the attack of chloride ions. Thus, the speed of the salt spray helped in the penetration of the saline solution inside the zinc coating layer and thus led to the destroyed (i.e., chemically modified and dissolved away) and peeling of parts of this protective layer. Because of this, the chloride ions content in the oxidized surface was 1.86 wt.%, which is also reduced by 82.4% of what it was in the uncoated sample. As for the welded-uncoated sample, we can notice an increase in the FeO value to 87.95wt.%, which is higher than the unwelded-uncoated sample value, as this sample did not withstand the attack of chloride ions, where the Cl_2O was high (9.96 wt.%) as well as the extension of the oxidized surface to include the welding area as well as shown also in *Fig. 6*, although carry out a stress removal treatment to get rid of the heat-affected zone (HAZ). It is possible that this is related to the presence of some micro-defects in the welding area results from the inefficiency of the welding process entirely along with the sample, which caused the appearance of rust in the welding surface.

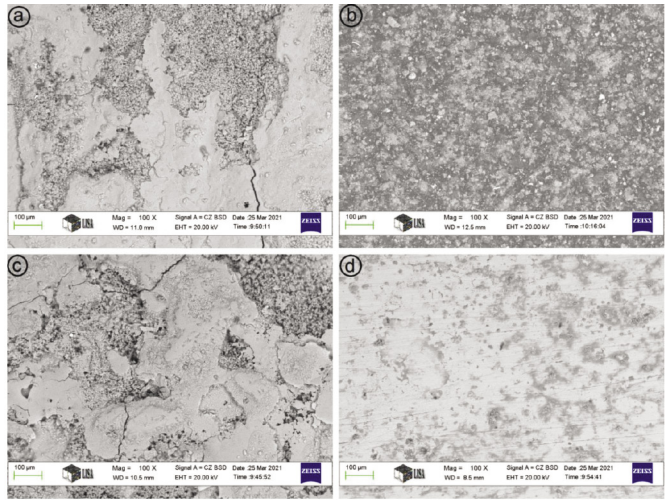

Fig. 5 SEM analysis for HSLA steel plates after exposure to 5% NaCl salt spray for 24 hours, (a) unwelded and uncoated sample, (b) unwelded and coated sample, (c) welded and uncoated sample, and (d) welded and coated sample
5. ábra A korroziós teszt után (24 óra, 5%-os NaCl sópermet) a HSLA acéllemezek SEM-elemzése: (a) hegesztés és bevonat nélküli minta, (b) hegesztés nélküli bevonatos minta, (c) hegesztett bevonat nélküli minta, (d) hegesztett és bevonatos minta

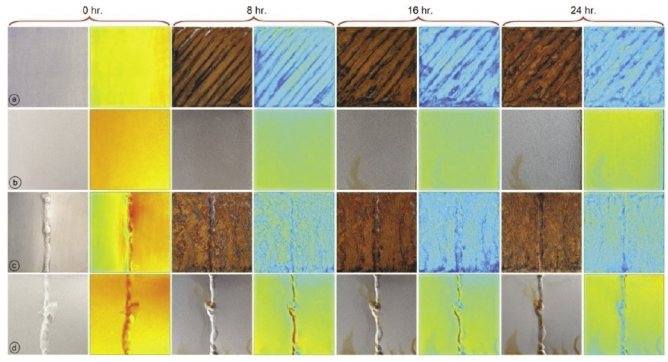

Fig 6. Surface topography and roughness measurements of high strength low alloy steel after 24 hours of exposure to 5% NaCl salt spray, (a) unwelded and uncoated sample, (b) unwelded and coated sample, (c) welded and uncoated sample, and (d) welded and coated sample
6. ábra HSLA acéllemezek felületi topográfiájának és érdességének mérési eredményei a korroziós teszt után (24 óra, 5%-os NaCl sópermet): (a) hegesztés és bevonat nélküli minta, (b) hegesztés nélküli bevonatos minta, (c) hegesztett bevonat nélküli minta,(d) hegesztett és bevonatos minta.

Components	EDX composition analysis, wt%			
	a	b	c	d
Cl_2O	10.55	1.86	9.96	2.99
SiO_2	2.25	1.75	1.54	1.5
MnO	0.67	0.76	0.55	0.94
FeO	86.53	4.75	87.95	6.98
ZnO	-	74.65	-	72.36

Table 3. The chemical composition of HSLA steel samples at different test durations under 5% NaCl salt spray analyzed by SEM-EDS, (a) unwelded-uncoated sample, (b) unwelded-coated sample, (c) welded-uncoated sample, and (d) welded-coated sample

3. táblázat HSLA acélminták kémiai összetétele SEM-EDS elemzéssel 5%-os NaCl sópermet után: (a) hegesztés és bevonat nélküli minta, (b) hegesztés nélküli bevonatos minta, (c) hegesztett bevonat nélküli minta, (d) hegesztett és bevonatos minta.

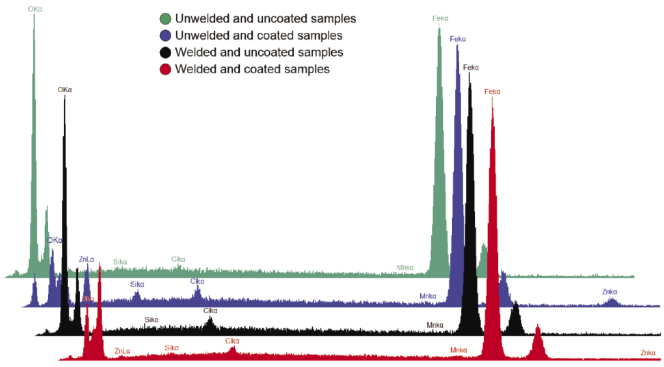

Fig. 7 EDX mapping analysis for HSLA steel plates

7. ábra HSLA acéllemezek EDX elemzése

As for the welded-coated sample, the oxidized surface was higher than in the unwelded-coated sample, where the FeO content was (6.98 wt.%) as we note from *Fig. 7* that despite the coating, the welding area has also oxidized. The reason for this is the rapid appearance of microcracks in the coating layer that covers the welding area, because it is uneven, so the superficial protuberances, no matter how small, will be prone to peeling the paint layer off it and being attacked by chloride ions. Therefore, we see that the proportion of Cl_2O is also high (2.99 wt.%) when compared with the Cl_2O proportion of the unwelded-coated sample. The EDS analysis of HSLA steel plates is shown in *Fig. 7*. Rust is made up of a variety of oxides, including hydrated oxides, oxyhydroxides, and other crystalline and amorphous compounds, although the major components are iron and oxide. As a result, determining the oxygen ratio in the rust layer can provide insight on corrosion process under similar exposure conditions. To further understand the initial corrosion, the chemical composition of the rust layer was examined after 24 hours period of salt spray exposure at typical locations and showed several corroded regions. General corrosion developed throughout the area, as seen in *Fig. 5*, and *Fig. 6*. Corrosion progressed in the sample un welded- uncoated and in the welded and uncoated sample, that was conformed also by peaks of oxygen in EDS analysis. The overall decrease in the corrosion rate in the samples with coating suggests that the corrosion delay was due to the Zinc coating layer because it decrease the harmful attack of chlorides. Corrosion in welded-uncoated sample in reality, when comparing the corrosion in the weld and HAZ zones, these zones is more severe due to the thermal effect because the welding temperature and these with effect of chlorides it will be weak to resist the corrosion [47].

3.2. Monitoring and evaluation of optical micrographs for the surface

Light optical micrographs for the surface of samples are presented in *Fig. 8*. The visual examination revealed that the corrosion initiated and started on the whole surface area of unwelded-uncoated and welded-uncoated samples. Inspection of the unwelded-coated and welded-coated samples upon corrosion initiation typically revealed one distinct corroding spot, which in some cases was surrounded by significantly smaller corrosion pits on the coating layer. The small corrosion pits were interpreted as micro defects where corrosion had initiated but could not reach stable pit growth (in contrast to the dominating corrosion state).

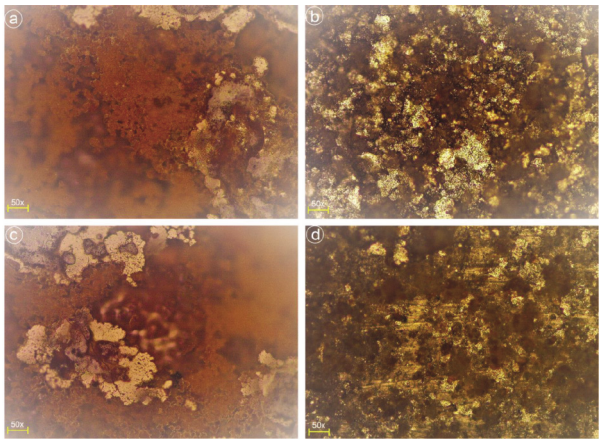

Fig. 8 Light optical micrographs of HSLA steel plates after 24 hours of exposure to 5% NaCl salt spray, (a) unwelded and uncoated sample, (b) unwelded and coated sample, (c) welded and uncoated sample, and (d) welded and coated sample

8. ábra A korróziós teszt után (24 óra, 5%-os NaCl sópermet) a HSLA acéllemezek fénymikroszkópos felvételei: (a) hegesztés és bevonat nélküli minta, (b) hegesztés nélküli bevonatos minta, (c) hegesztett bevonat nélküli minta, (d) hegesztett és bevonatos minta

3.3 Surface topography changes in roughness

The change in surface roughness on the HSLA steel plates surface was mentioned in *Fig. 6*. Before the salt spray test, the surface of the samples has a typical ground topography. However, this simple regular surface pattern soon changes, where more irregular surface and complex topography appear, depending on the type of sample and the duration of exposure to the saline solution. This new topography represents rust, as well as changes to the coating layer. In the stage of the appearance of rust and the effect of the coating layer due to saline solution, the surface roughness will change drastically, as its values will rise, as expected, as shown in the *Fig. 9* and *10*, which represent roughness average and core roughness depth respectively. Uncoated samples generally have the highest roughness rates, and welded samples are the highest despite being coated. Unwelded and coated sample showed the lower roughness values during the different test durations under 5% NaCl salt spray; also welded and coated sample showed slightly higher roughness values comparing with sample unwelded one. These samples (coated) appeared good resistance for corrosion after 24 hours under 5% NaCl salt spray because the zinc coating layer improved the ability to resist the attack of chloride ions and that will lead to progress in the corrosion process slowly. In addition, the values of the roughness depth parameters (Sk) are on average more than twice as high as their roughness average equivalent

(Sa) on the corroded surfaces. One possible reason for this can be that the corrosion appears crater-like at certain points on the surface and therefore has a high surface in homogeneity, which is better detected by roughness depth characteristics.

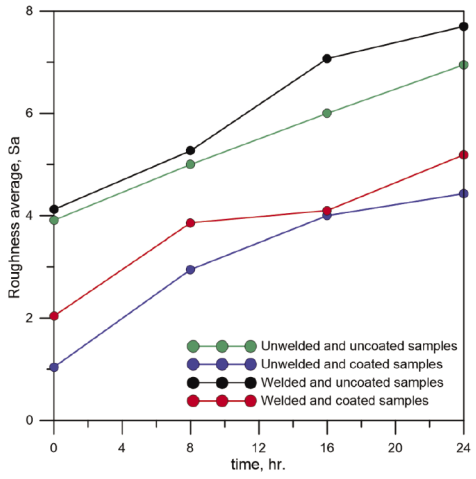

Fig. 9 Roughness average (Sa) values for HSLA steel plates at different test durations under 5% NaCl salt spray
9. ábra Különböző idejű sópermet (5% -os NaCl) teszt után a HSLA acélemezek átlagérdessége (Sa)

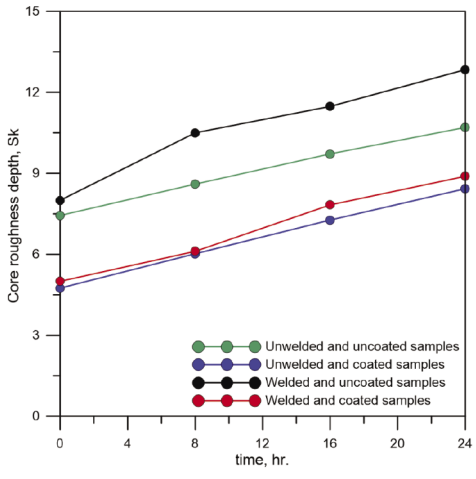

Fig. 10 Core roughness depth (Sk) values for HSLA steel plates at different test durations under 5% NaCl salt spray
10. ábra Különböző idejű sópermet (5% -os NaCl) teszt után a HSLA acélemezek magmagassága (Sk)

4. Conclusions

The oxidized areas spread on the whole surface of the uncoated samples after 8 hours after exposure to the salt spray; this chemical attack also caused significant changes in the surface topography. The percentage of zinc compounds in the case of unwelded-coated samples was higher than that of welded-coated samples by 3.07%, indicating that part of the coating layer has peeled off the welding area, which contributed to its exposure to the attack of chloride ions. Corrosion points appear on the weld area extensively even though they are coated, and stress relieving heat treatment is applied. We believe this behavior may result from the inefficiency of the welding process along the welded surface through the appearance of micro-cracks after welding or the entry of oxygen due to the shallowness of the inert gas which caused poor insulation and full enclosing of the welding area from the outside atmosphere. Therefore, manufacturers must pay attention to these areas and ensure the total efficiency of the welding to provide maximum safety in vehicles. The lowest rates of surface roughness were in the unwelded and coated samples, where the roughness of these samples was less than the welded and coated samples by 17.2% and 5.5% for the roughness average and core roughness depth, respectively. Also, the intensity of the roughness rate after exposure to salt spray varies in the case of the unwelded-uncoated samples and welded-uncoated samples, where the roughness average and core roughness depth were higher in the case of welded-uncoated by 10.8% and 20, respectively than unwelded-uncoated samples, after 24 hours exposure to the saline spray. Concentrations of oxygen and iron oxide (FeO) in welded samples, whether coated or uncoated, are higher than those unwelded ones, which indicates that the salt spray has been penetrated the coating layer earlier than the unwelded ones. The irregular diverse topography of the welding area plays a pivotal role in increasing the coating removal rate from them, making this area susceptible to corrosion, and this is also observed from the low content of ZnO in the welded samples, which is 3.16% less than its unwelded-coated counterparts.

Acknowledgements

We would like to extend our thanks and appreciation to Mr. Lassú Gábor and Mr. Kovács Árpád at the University of Miskolc for their valuable help in salt spray test and SEM measurements.

Reference

[1] Vengosh A., Salinization and saline environments, Chapter 9, In Holland, H.D., Turekian, K.K. (eds.) Treatise on Geochemistry, 2nd edition, Volume 11: Environmental Geochemistry, Elsevier Ltd., pp. 325-378, (2014). https://doi.org/10.1016/B978-0-08-095975-7.00909-8
[2] Kelly V.R., Findlay S.E.G., Schlesinger W.H., Menking K., Morrill A., Road salt moving toward the solution, Special Report, Cary Institute of Ecosystem Studies, USA, (2010). https://www.caryinstitute.org/sites/default/files/public/reprints/report_road_salt_2010.pdf
[3] Evans M., Frick Ch., The effects of road salts on aquatic ecosystems, National Water Research Institute, Series No. 02-308, Canada, (2001). http://scec.ca/pdf/the_effects_road_salts.pdf
[4] Green S.M., Machin R., Cresser M.S., Effect of long-term changes in soil chemistry induced by road salt applications on N-transformations in roadside soils, Environmental Pollution, Vol.152, Issue.1, pp.20-31, (2008). https://doi.org/10.1016/j.envpol.2007.06.005
[5] Novotny E., Murphy D., Stefan H., Road salt effects on the water quality of lakes in the twin cities metropolitan area, St. Anthony Falls Laboratory, Project Report No. 505, Minneapolis, Minnesota, (2007). https://conservancy.umn.edu/bitstream/handle/11299/115334/1/pr505.pdf
[6] Hintz W.D., Fay L., Relyea R.A., Road salts, human safety, and the rising salinity of our fresh waters, Frontiers in Ecology and the Environment,Vol.20, Issue.1, pp.22-30, (2022). https://doi.org/10.1002/fee.2433
[7] Kostka A., Strzebońska M., Sobczyk M., Zakrzewska M., Bochenek A., The effect of de-icing roads with salt on the environment in Krakow (Poland), Geology, Geophysics & Environment, Vol.45, Issue.3, pp.195-205, (2019). https://doi.org/10.7494/geol.2019.45.3.195
[8] Szklarek S., Górecka A., Wojtal-Frankiewicz A., The effects of road salt on freshwater ecosystems and solutions for mitigating chloride pollution - A review, Science of The Total Environment, Vol.805, pp.150289, (2022). https://doi.org/10.1016/j.scitotenv.2021.150289
[9] Wrochna M., Małecka-Przybysz M., Gawrońska H., Effect of road de-icing saltswith anti corrosion agents on selected plant species, Acta Scientiarum Polonorum, Hortorum Cultus, Vol.9, No.4, pp.171-182, (2010). https://czasopisma.up.lublin.pl/index.php/asphc/article/view/3442

[10] Hernandez B., The Effects of road salt on cars & how to protect your vehicle from salt damage, Brian's Auto Detailing, LLC, (2019). https://www.briansautodetailing.com/post/the-effects-of-road-salt-on-cars-how-to-protect-your-vehicle-from-salt-damage
[11] Buchheit R.G., Corrosion resistant coatings and paints, In: Kutz M. (ed.) Handbook of environmental degradation of materials, 2nd edition, William Andrew, USA, pp. 539-568, (2013). https://doi.org/10.1016/B978-1-4377-3455-3.00018-3
[12] Wood F.O., Motor-vehicle corrosion from deicing salt, Transportation Research Record, Vol.762, pp.32-36, (1980). https://onlinepubs.trb.org/Onlinepubs/trr/1980/762/762-007.pdf
[13] Petkuviene J., Paliulis D., Experimental research of road maintenance salts and molasses ("safecote") corrosive impact on metals, Journal of Environmental Engineering and Landscape Management, Vol.17, Issue.4, pp.236-243, (2009). https://doi.org/10.3846/1648-6897.2009.17.236-243
[14] Xi Y., Olsgar P. J., Effects of de-icing agents (magnesium chloride and sodium chloride) on corrosion of truck components, Report No. CDOT-DTD-R-00-10, Colorado Department of Transportatio, USA, (2000). https://www.codot.gov/programs/research/pdfs/2000/truckcomponents.pdf
[15] ISO 26262, Road vehicles-functional safety, International Organization for Standardization-ISO, (2018). https://www.iso.org/obp/ui/#iso:std:iso:26262:-1:ed-2:v1:en
[16] Solonshchikov P., Moshonkin A., Determination of safety parameters for cars and tractors, Transportation Research Procedia, Volume 61, pp.492-498, (2022). https://doi.org/10.1016/j.trpro.2022.01.080
[17] Kitagawa Y., Pal Ch., Evaluation of vehicle body stiffness and strength for car to car compatibility, SAE Technical Paper 2001-01-3098, (2001). https://doi.org/10.4271/2001-01-3098.
[18] Volvo XC60 safety cage, Volvo Car Corporation, (2009). https://www.media.volvocars.com/global/en-gb/media/photos/14629
[19] Vasilash G.S., The Volvo XC60: Stylish, Swedish & Safe, Technical Report, Gardner Business Media, Inc., (2009). https://www.gardnerweb.com/articles/the-volvo-xc60-stylish-swedish-safe
[20] Arno J., Matthias B., New cars-new materials, materials & design, Vol.18, Issues.4-6, pp.203-209, (1997). https://doi.org/10.1016/S0261-3069(97)00049-6
[21] Cheon S. S., Lee D. G., Jeong K. S., Composite side door impact beams for passenger cars, Composite Structures, Vol.38, Issues.1-4, pp.229-239, (1997). https://doi.org/10.1016/S0263-8223(97)00058-5
[22] Sivanura K., Umananda K.V., Pai D., Advanced materials used in automotive industry-a review, AIP Conference Proceedings, Vol.2317, pp.020032, (2021). https://doi.org/10.1063/5.0036149
[23] Abdulsada Sh.A., Corrosion inhibitors :principles and application, 1st Edition, LAP- LAMBERT Academic Publishing, Germany, (2014).
[24] Henriksson F., Introducing new materials in the automotive industry-managing the complexity of introducing new materials in existing production systems, Ph.D. dissertation, Linköping University, Sweden, (2017). https://liu.diva-portal.org/smash/get/diva2:1155571/FULLTEXT02.pdf
[25] Johnson M.C., Sullivan J.L., Lightweight materials for automotive application: an assessment of material production data for magnesium and carbon fiber, Technical Report, Argonne National Laboratory, USA, (2014). https://doi.org/10.2172/1172026
[26] Abdulsada Sh.A., Al-Mosawi A.I., Hadi A.A., studying the effect of eco-addition inhibitors on corrosion resistance of reinforced concrete, Bioprocess Engineering, Vol.1, No.1, pp.81-86, (2017). https://doi.org/10.11648/j.be.20170103.14
[27] Hovorun T. P., Berladir K.V., Pererva V.I., Rudenko S.G., Martynov A. I., Modern materials for automotive industry, Journal of Engineering Sciences, Vol.4, Issue.2, pp. F8-F18, (2017). https://doi.org/10.21272/jes.2017.4(2).f8
[28] Al-Sultani K.F., Abdulsada Sh.A., Improvement corrosion resistance of low carbon steel by using natural corrosion inhibitor, International Journal of Advanced Research, Vol.1, Issue.6, pp. 239-243, (2013). https://www.journalijar.com/uploads/2013-06-26_160757_152.pdf
[29] Hosking N.C., Next generation corrosion protection for the automotive industry, PhD dissertation, University of Nottingham, Uk, (2007). http://eprints.nottingham.ac.uk/14514/1/585527.pdf
[30] Hall J.N., Fekete J.R., Steels for auto bodies: a general overview, In: Rana, R., Singh, S.B. (eds.) Automotive steels: design, metallurgy, processing and applications, Woodhead Publishing, USA, pp. 19-45, (2017). https://doi.org/10.1016/B978-0-08-100638-2.00002-X
[40] Samek L., Krizan D., Steel - material of choice for automotive lightweight applications, 21st International Conference on Metallurgy and Materials, Brno, Czech Republic, , pp.1-6, (2012). http://metal2012.tanger.cz/files/proceedings/02/reports/551.pdf
[41] Li Y., Lin Z., Jiang A., Chen G., Use of high strength steel sheet for lightweight and crashworthy car body, Materials and Design Vol.24, Issue.3, pp.177-182, (2003). https://doi.org/10.1016/S0261-3069(03)00021-9
[42] Cornette D., Hourman T., Hudin O., Laurent J., Reynaert A., High strength steels for automotive safety parts, SAE 2001World Congerss, Detroit, Michigan, USA, pp.0078, (2001). https://doi.org/10.4271/2001-01-0078.
[43] Abdulsada Sh.A., Al-Mosawi A.I., Török T.I., Testing the inhibition potential of fenugreek seed powders on steel rebar samples immersed in aqueous NaCl solution, Proceedings of MultiScience - XXXI. MicroCAD International Multidisciplinary Scientific Conference, University of Miskolc, Hungary, 2017, pp.1-6, (2017). https://doi.org/10.26649/musci.2017.026
[44] Schulz U., Trubiroha P., Schernau U., Baumgart H., The effects of acid rain on the appearance of automotive paint systems studied outdoors and in a new artificial weathering test, Progress in Organic Coatings, Vol.40, Issue.1-4, pp.151-165, (2000). https://doi.org/10.1016/S0300-9440(00)00138-7
[45] Akafuah N.K., Poozesh S., Salaimeh A., Patrick G., Lawler K., Saito K., Evolution of the automotive body coating process-a review, Coatings, Vol.6, Issue.2, 2016, pp.24, (2016). https://doi.org/10.3390/coatings6020024
[46] Abdulsada Sh.A., Török T.I., Fazakas É., Preliminary corrosion testing of steel rebar samples in 3.5% NaCl solution with and without a green inhibitor, Építőanyag-Journal of Silicate Based and Composite Materials, Vol.70, No.2, pp. 48-53, (2018). https://doi.org/10.14382/epitoanyag-jsbcm.2018.10
[47] Zinc coatings: a comparative analysis of process and performance characteristics, Technical Report, American Galvanizers Association, (2011). https://galvanizeit.org/uploads/publications/Zinc_Coatings.pdf
[48] Rocca E., Jacques S., Electrochemical coating of zinc carboxylate: a new protection for Zinc in atmospheric conditions, Surface and Coatings Technology, Vol.429, pp.127940, (2022). https://doi.org/10.1016/j.surfcoat.2021.127940
[49] Amirudin A., Thierry D., Corrosion mechanisms of phosphated zinc layers on steel as substrates for automotive coatings, Progress in Organic Coatings, Vol.28, Issue.1, pp.59-75, (1996). https://doi.org/10.1016/0300-9440(95)00554-4
[50] Petrova L., Demin P., Kolenko N., Luzhnov Y., Increasing the reliability of low-carbon cold-resistant steel elements by diffusion zinc coating methods, Transportation Research Procedia, Vol.57, pp.421-429, (2021). https://doi.org/10.1016/j.trpro.2021.09.069
[51] ISO 9227-3, Corrosion tests in artificial atmospheres- salt spray tests, Switzerland, International Organization for Standardization-ISO, (2017).
[52] ISO 21920-2, Geometrical product specifications (GPS) -Surface texture: Profile -Part 2: Terms, definitions and surface texture parameters, Switzerland, International Organization for Standardization-ISO, (2021). https://www.iso.org/obp/ui/#iso:std:iso:21920:-2:ed-1:v2:en
[53] ISO 21920-3, Geometrical product specifications (GPS)-Surface texture: Profile- Part 3: Specification operators, Switzerland, International Organization for Standardization-ISO, (2021). https://www.iso.org/obp/ui/#iso:std:iso:21920:-3:ed-1:v1:en
[54] ISO 25178-2, Geometrical product specifications (GPS)- Surface texture: Areal- Part 2: Terms, definitions and surface texture parameters, Switzerland, International Organization for Standardization-ISO, (2021). https://www.iso.org/obp/ui/#iso:std:iso:25178:-2:ed-1:v1:en
[55] Alcántara J., Fuente D., Chico B., Simancas J., Díaz I., Morcillo M., Marine atmospheric corrosion of carbon steel: a review, Materials, Vol. 10, Issue. 4, 2017, pp.406, (2017). https://doi.org/10.3390/ma10040406
[56] Choi Y.Y., Kim M.H., Corrosion behaviour of welded low-carbon steel in the arctic marine environment, RSC Advances, Vol.8, Issue.53, pp. 30155-30162, (2018). https://doi.org/10.1039/C8RA05371E

Ref.:
Abdulsada, Shaymaa Abbas– **Al-Mosawi**, Ali I.: *Corrosion behaviour and surface topography for steel plates used in automotive industry exposed to salty corrosive thermo-accelerated medium*
Építőanyag – Journal of Silicate Based and Composite Materials, Vol. 74, No. 6 (2022), 218–223. p.
https://doi.org/10.14382/epitoanyag-jsbcm.2022.31

Investigation of the influence of temperature-time regimes on the morphological features of slawsonite ceramics

George LISACHUK
Doctor of Sciences, full Professor. Specialist in material sciences of resource saving and energy-saving technologies, new structural ceramic materials and coatings. Head of Research department of NTU "KhPI".

Ruslan KRYVOBOK
Ph.D, Senior researcher. Specialist in material sciences of new special-purpose ceramic materials and coatings. Deputy Head of Scientific and Research Part NTU "KhPI"

Valentyna VOLOSHCHUK
Ph.D. student, NTU "KhPI", Department of technology of ceramics, refractories, glass and enamels. Specializes in the study of radiotransparent ceramic materials.

Olena LAPUZINA
Candidate of pedagogical science. Fields of interests: innovative teaching methods, distance learning; interdiscliplinary coordination; theory and practice of teaching business ethics.

George V. LISACHUK ▪ National Technical University "Kharkiv Polytechnic Institute", Ukraine ▪ lisachuk @ kpi.kharkov,
Ruslan V. KRYVOBOK ▪ National Technical University "Kharkiv Polytechnic Institute", Ukraine ▪ krivobok491@gmail.com,
Valentyna V. VOLOSHCHUK ▪ National Technical University "Kharkiv Polytechnic Institute", Ukraine ▪ valenty93vol@gmail.com,
Olena M. LAPUZINA ▪ National Technical University "Kharkiv Polytechnic Institute", Ukraine ▪ elapuzina@gmail.com

Érkezett: 2022. 07. 04. ▪ Received: 04. 07. 2022. ▪ https://doi.org/10.14382/epitoanyag-jsbcm.2022.32

Abstract
The paper considers a new technology for obtaining ceramic materials based on slawsonite, which is a two-stage one. The first stage is the synthesis of the slawsonite phase and the grinding of the synthesized material. The second stage is the formation of raw material by the method of slip casting into plaster molds and the subsequent firing of the products. The effect of temperature-time regimes on the properties of slawsonite ceramics has been studied. Changeable technological parameters: firing temperature of products – 1,350 °C and 1,400 °C, exposure at maximum temperature – 2 and 4 hours. The morphology and phase features of the samples were studied by X-ray phase analysis and scanning electron microscopy. Regularities of changes in physical and mechanical properties depending on the temperature and duration of firing of experimental ceramics are established. It is proved that with an increase in the duration of firing of samples, the values of water absorption and open porosity decrease and the density of slawsonite ceramics increases. The mechanical and dielectric properties of experimental ceramics are experimentally studied, the values of which are in the ranges ε = 5.8 - 13.2; σ = 140 - 390 MPa.
Keywords: Slawsonite, radio-transparent materials, morphology, phase features, mechanical properties, dielectric properties
Kulcsszavak: Slawsonit, rádiótranszparens anyagok, morfológia, fázisjellemzők, mechanikai tulajdonságok, dielektromos tulajdonságok

1. Introduction

In wartime, the development of new types and classes of weapons is essential to ensure the state integrity of Ukraine. The development of new generations of guided air-to-air, air-to-surface missiles and anti-aircraft missiles requires the development and implementation of a wide range of materials with improved physicochemical, mechanical, thermal and electrophysical characteristics.

The interest of developers in the problem of creating radio-transparent ceramic materials with operating temperatures up to 1,500 °C is obvious. As a rule, materials for this purpose are powder ceramics based on refractory compounds. Powder technology in comparison with a sitall technology provides the increased stability and reproducibility of physical and chemical properties of materials. Modern technologies allow to obtain a wide range of properties through the manufacture of materials by modifying them with various additives to add special properties.

The relevance of the direction and research as a whole is in finding materials that can satisfy a set of specific requirements for the manufacture of aircraft elements and investigate the dependence of the influence of technological parameters on the structure that determines its properties.

2. Analysis of literature data and problem statement

Slawsonite ceramics is a fairly new and promising material for obtaining radio-transparent fairings. It belongs to electrical ceramics. Strontium anorthite $SrAl_2Si_2O_8$ belongs to the feldspar group of minerals, has a high melting point (1,765 °C), reduced thermal expansion coefficient ($6.5 \cdot 10^6$ 1/degree), low values of dielectric constant (6.0-7.0) and tangent. dielectric loss angle ($11.0 - 50.0 \cdot 10^{-4}$) in a wide temperature and frequency ranges [1-4]. The properties of slawsonite ceramics depend on the chemical and phase composition, macro- and microstructures, as well as on the technological methods of manufacturing products [5-7].

In the USA, to create more advanced high-temperature radio-transparent materials, glass-ceramics based on monoclinic strontium and barium aluminosilicates are considered, which has the following characteristics: dielectric constant ε = 6.55 - 7.0; dielectric loss tangent tan δ = (8 - 25) · 10^{-4}, for strontium-containing compositions: ε = 6.16 - 6.77 and tan δ = (11 - 50) · 10^{-4} at 1,100 °C [8,9].

In works [10, 11], densely sintered materials based on strontium-anorthite ceramics with low temperature coefficient of linear expansion (TKLE) values (32.0 - 33.4) · 10^{-7} $deg.^{-1}$ were obtained, which causes their high heat resistance (not lower than 850 °C). High density values (2.40 - 2.50 g/cm^3) and mechanical compressive strength limits (237 - 246 MPa) are observed. In turn, the dense microstructure allows to achieve high dielectric values (ε = 4.4 - 4.8; tgδ = 0.005 - 0.007) at a frequency of 10 GHz.

In South Korea, the solution to the problem of obtaining ceramic materials containing only the stable monoclinic form of slawsonite was achieved at Daejin University (Department of Materials Science and Engineering), which made it possible to obtain glass-ceramic composite materials with high radio transparency, strength, and low TKLE values. Glass ceramics containing monoclinic strontium anorthite were obtained based on the stoichiometric composition after crystallization at 1,100 °C for 1 hour or at a temperature of ≥ 1184 °C for a shorter period [12, 13].

However, the production of glass-ceramic materials based on aluminosilicate systems using network technology is an energy-intensive process (glass melting temperature is about 1,600 °C – 1,700 °C), and also introduces a limitation on the complexity of the forms of finished products. Therefore, it is important to take into account the availability and simplicity of the technology for obtaining the final product.

NTU "KhPI" performs works [14-16] on obtaining radio-transparent ceramics using ceramic technology by semi-dry pressing. The authors of the works investigated possible ways of formation and conditions of low-temperature synthesis of the slawsonite phase. In [16], slawsonite ceramics were obtained during single-stage firing in an induction laboratory furnace at a temperature of 1,550 °C with holding at this temperature for 5 hours. However, in this work, when forming samples, the semi-dry pressing method was used, which does not allow obtaining products of complex shape.

In modern conditions, in most areas of engineering and technology, they are most promising for use as structural products with an intergranular and uniform structure. All the most important properties of products are determined, as a rule, by the microstructure and phase composition of the material, which are determined by the structure of the initial powder, the firing mode, etc. Therefore, within the framework of this study, an important task is to develop technological parameters for creating a material that can meet a number of basic requirements for products obtained using slip casting.

3. The purpose and objectives of the study

The purpose of this work is to study the influence of technological parameters on the morphological features of slawsonite ceramics. To achieve these goals, it is necessary to solve the following tasks:

- to develop technological parameters for obtaining slawsonite radio-transparent ceramics by the method of water slip casting;
- to study the structural and phase features of the obtained ceramic samples;
- to study the operational and dielectric properties of the obtained samples, which determine the quality of finished products.

4. Materials and methods

Slawsonite was chosen as the main phase, which according to the level of electrophysical properties satisfies the requirements for radio-transparent materials and allows to obtain materials with a low reflection coefficient of radio waves and high heat resistance. G-00 alumina, strontium carbonate and quartz sand were used as raw materials, and a eutectic additive of lithium carbonate and stanum oxide was used to intensify the synthesis process.

Samples were prepared using a two-stage technology. In the laboratory, the mixture was homogenized by grinding raw materials in a ball mill with their subsequent passage through a sieve № 015. The resulting press powder was moistened with a solution of carboxymethyl cellulose («UGUR SELULOZ KIMYA», Turkey) moisture content - 8%. Then the formation of briquettes with dimensions of 50×20×50 mm from semi-dry masses was carried out by pressing the mixture on a manual hydraulic press MHP-10 under a pressure of 20 MPa. Drying in the oven was carried out at a temperature of 80 °C, to a residual humidity of not more than 1.0%. The synthesis in a muffle furnace at a rate of 10 degrees/min at a maximum firing temperature of 1250 °C with a holding time of 2 hours was performed. The synthesis of the synthesized substance took place for 10 minutes in the planetary mill Retch, before passing through a sieve № 0063 and the residue on it no more than 1.0%.

The slurry from the synthesized substance with a moisture content of 30% was obtained in a ball mill at a ratio of substance: ceramic layers 1:3, with the addition of a diluent Dolapix PC 67. To obtain the raw product a ready slurry was poured into gypsum mold. Drying of the raw material was carried out in an oven to a residual moisture of not more than 1.0%. The firing of the dried raw material was carried out in a silitic furnace Nabertherm in an accelerated mode: the rate of temperature accumulation – 12 - 15 degrees/min, the maximum firing temperature was 1350 °C and 1400 °C; exposure at maximum temperature – 2 and 4 hours. The fired products were subjected to machining.

Determination of dielectric properties was carried out on the immittance meter E 7 – 8 at a frequency of 1 kHz. Samples with a diameter of 37 mm and a thickness of 5 mm and an electrode diameter of 30 mm were used to determine the dielectric constant. To ensure a tight fit of the electrodes, the samples for research were ground. With the measured values of the electrical capacity of the samples, dielectric permeability was determined.

Determination of the apparent density and water absorption of the samples was carried out in a method of hydrostatic weighing in water.

The phase composition of the experimental samples was determined using the method of X-ray phase analysis (XRD). X-ray diffractograms were taken on a Dron-3M diffractometer with CuK_α – by radiation and a nickel filter under constant conditions of its operation.

The study of the microstructure of the samples and the morphology of the surface of their faults was carried out by direct scanning electron microscopy using a scanning electron microscope PhenomPro Desktop SEM (Thermo Fisher Scientific, USA) with an accelerating voltage of 15 kV.

5. Results and discussion

Ceramics synthesized at a temperature of 1250 °C with a holding time of 2 hours were investigated by X-ray phase analysis to determine the completeness of the reaction of formation of the slawsonite phase. The results of X-ray phase analysis are shown in *Fig. 1*.

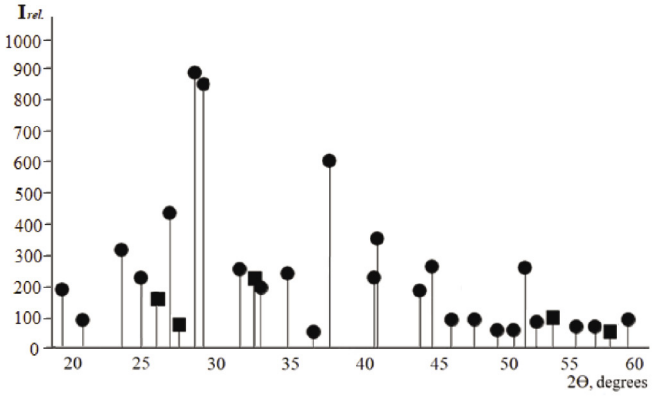

● – *slawsonite* ($SrAl_2Si_2O_8$), ■ – *strontium metasilicate* ($SrSiO_3$)

Fig. 1 Bar radiograph of slawsonite synthesized at a temperature of 1250 °C
1. ábra 1250 °C hőmérsékleten szintetizált slawsonit röntgenfelvétele

At the synthesis temperature of 1250 °C (*Fig. 1.*) the data indicate that the reaction of slawsonite synthesis is not complete. In addition, to the peaks of the crystalline phase of slawsonite, insignificant peaks of the intermediate compound strontium metasilicate are observed. However, there are no peaks of carbonates, which indicates the complete course of the dissociation reaction of the compound $SrCO_3$. Due to this reaction, the synthesis of the phase is accompanied by a large fire shrinkage (up to 20%) and can lead to defects during firing of products by one-stage technology. In connection with the above, this research uses a two-stage ceramic technology for antenna fairings.

To conduct experiments to establish the best technological parameters for the production of fairings from slawsonite ceramics in the framework of this work, firing temperature of samples – 1350 °C and 1400 °C, and exposure time at maximum firing temperature – 2 and 4 hours were selected as the variable technological parameters. To compare the samples, their physical-mechanical and dielectric properties were studied. The result was the arithmetic mean of three parallel tests. The results of studies of samples of slawsonite ceramics are shown in *Table 1*.

The fired samples were characterized by the absence of visible defects. From the obtained data we could see that with increasing the firing time from 2 to 4 hours, the indicators of both physical-mechanical and dielectric properties of slawsonite ceramics improve.

T_{firing}, °C	τ_{firing}, hours	Water absorption, %	Open porosity, %	Apparent density, g/cm³	Bending strength, MPa	Apparent dielectric permittivity
1350	2	5.2	13.1	2.52	139	13.2
	4	0.3	0.7	2.85	392	5.8
1400	2	5.1	12.9	2.53	175	11.6
	4	4.2	10.8	2.60	219	9.7

Table 1. Physical-mechanical and dielectric properties of samples of slawsonite ceramics
1. táblázat A slawsonit kerámiaminták fizikai-mechanikai és dielektromos tulajdonságai

The best indicators of physical and mechanical properties of the test samples are obtained at a firing temperature of 1350 °C and exposure for 4 hours (water absorption – 0.3%, apparent density – 2.85 g/cm³, porosity – 0.7%, flexural strength – 392 MPa), which indicates a high density of the cast workpiece. The samples were also characterized by low apparent dielectric permittivity ε – 5.8, which meets the requirements for radio-transparent materials. The indicators of the investigated properties are close in values to the indicators of the samples of slawsonite ceramics obtained by the method of semi-dry pressing under the same conditions of the firing temperature – 1350 °C.

Structural and phase features of the obtained ceramics were studied by X-ray diffraction and scanning electron microscopy. The results of qualitative X-ray phase analysis showed that at firing temperatures above 1350 °C in all samples there is only the phase $SrAl_2Si_2O_8$, which indicates the completeness of the reactions of formation of the main phase. For example, *Fig. 2.* shows a bar-radiograph of samples obtained at a firing temperature of 1350 °C.

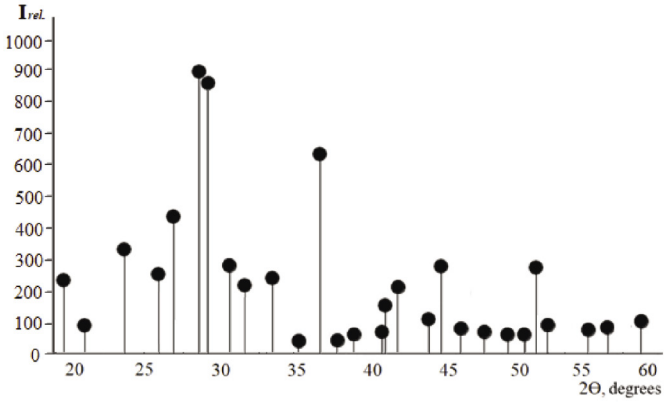

● – *slawsonite* ($SrAl_2Si_2O_8$)

Fig. 2 Bar radiograph of slawsonite ceramics obtained at firing temperature of 1350 °C
2. ábra 1350 °C-os égetési hőmérsékleten készült slawsonite kerámiák röntgenfelvétele

Morphological features of the surfaces of the obtained slawsonite ceramics were investigated using scanning electron microscopy. Photomicrographs of fractures of samples fired at temperatures of 1350 °C and 1400 °C and with exposure for 2 and 4 hours are shown in *Fig. 3-6.*

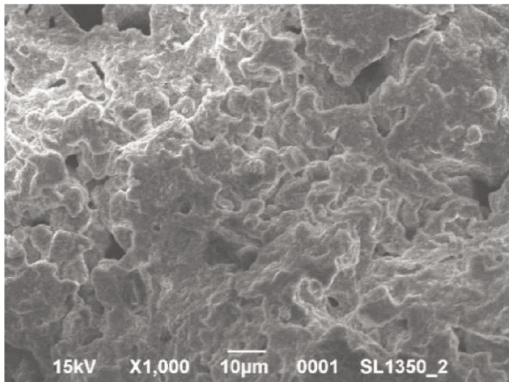

a)

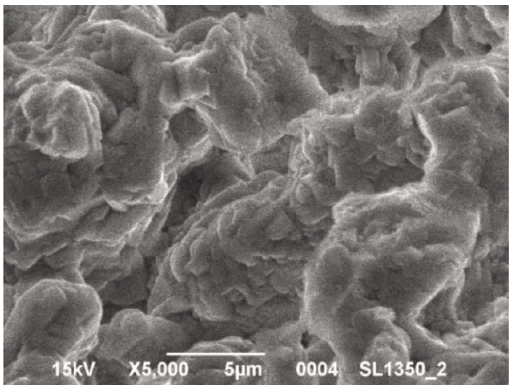

b)

Fig. 3 Microstructure of samples of slawsonite ceramics at a holding time of 2 hours at a temperature of 1350 °C

3. ábra Az 2 óra hőtartással 1350 °C hőmérsékleten készített slawsonit kerámiaminták mikroszerkezete

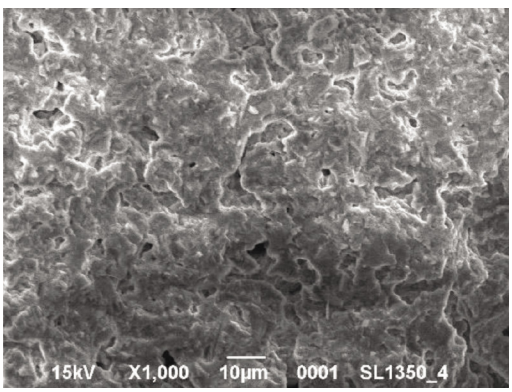

a)

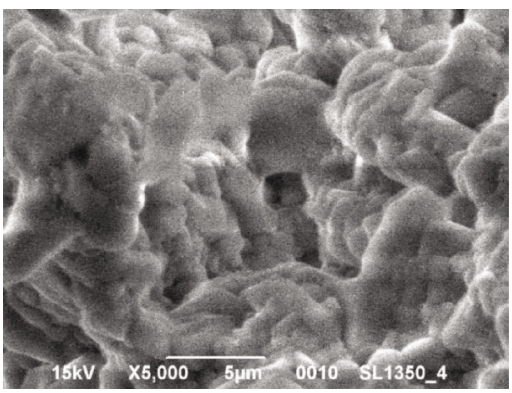

b)

Fig. 4 Microstructure of samples of slawsonite ceramics at a holding time of 4 hours at a temperature of 1350 °C

4. ábra Az 4 óra hőtartással 1350 °C hőmérsékleten készített slawsonit kerámiaminták mikroszerkezete

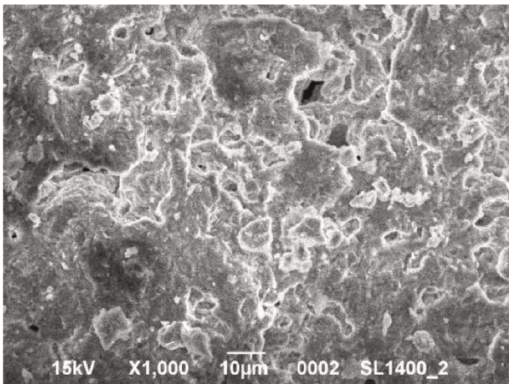

a)

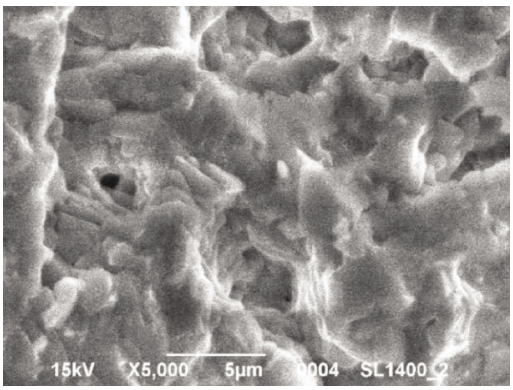

b)

Fig. 5 Microstructure of samples of slawsonite ceramics at a holding time of 2 hours at a temperature of 1400 °C

5. ábra Az 2 óra hőtartással 1400 °C hőmérsékleten készített slawsonit kerámiaminták mikroszerkezete

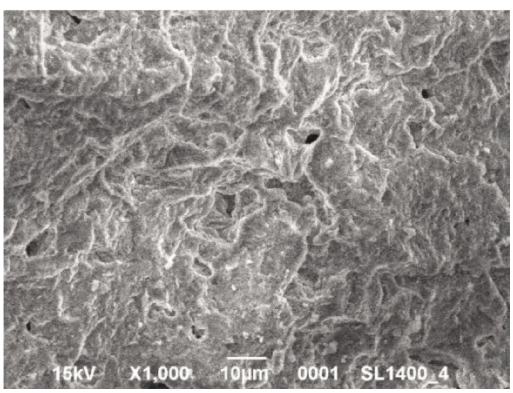

a)

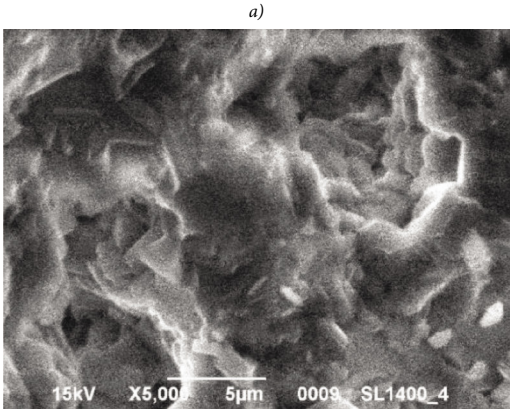

b)

Fig. 6 Microstructure of samples of slawsonite ceramics at a holding time of 4 hours at a temperature of 1400 °C

6. ábra Az 4 óra hőtartással 1400 °C hőmérsékleten készített slawsonit kerámiaminták mikroszerkezete

Images *Fig. 3 (a), 4 (a), 5 (a), 6 (a)* allow us to assess the natural roughness of the chip surface, the porosity of the samples and the homogeneity of the material structure. In the images *Fig. 3 (b), 4 (b), 5 (b), 6 (b)* starting from 1350 °C we could see the active growth of the crystalline structure of slawsonite.

In samples with a holding time of 2 hours at a firing temperature of 1350 °C, the presence of pores with a size of about 10 μm, which significantly impairs the mechanical properties of the samples. With increasing exposure time to 4 hours, we see a densely sintered, homogeneous structure with pores of no more than 1-2 μm and a clearer structure of slawsonite, which also reduces the dielectric permittivity. Based on the results of the study of the microstructure, we assumed that increasing the holding time to 4 hours has a positive effect on the operational and dielectric properties of the obtained ceramics.

According to the results of complex researches it is established that the material acquires the best properties at firing temperature of 1350 °C and endurance at maximum temperature for 4 hours in the studied area of technological parameters. Ceramic nose fairings obtained according to the recommended technological parameters of production have the following properties: water absorption – 0.7 - 0.9%, apparent density – 2.6 - 2.8 g/cm^3, porosity – 1.6 - 2.2%, limit bending strength – 340 - 360 MPa and apparent dielectric permittivity – 6.5 - 7.2.

The obtained materials based on slawsonite meet the requirements of the standard GOST 20419-83 (subgroup 420) and can be used for the creation of radio-transparent ceramics and the manufacture of radio-transparent ceramic nose fairings. It is established that according to the values of these characteristics, the materials belong to the radio-transparent ceramics and can be used in the aerospace industry for the manufacture of individual parts.

6. Conclusions

As a result of the work, the morphological features of slawsonite ceramics were investigated. The influence of technological parameters on the physical-mechanical and dielectric properties of the obtained ceramics is studied. According to the results of complex researches, the following technological parameters of production of radio-transparent ceramic nasal fairings on the basis of slawsonite are recommended: the first stage – synthesis at a temperature of 1250 °C, endurance time at the maximum temperature – 2 hours; the second stage is the formation of the fairing by the method of slip casting into gypsum molds, the firing temperature of the fairing – 1350 °C, the holding time at maximum temperature – 4 hours.

Ceramic nose fairings obtained by optimal technological parameters have the following properties: water absorption – 0.7 - 0.9%, apparent density – 2.6 - 2.8 g/cm^3, porosity – 1.6 - 2.2 %, strength bending – 340 - 360 MPa and apparent dielectric permittivity – 6.5 - 7.2.

Developed materials based on the slawsonite phase $SrAl_2Si_2O_8$ meet the requirements of GOST 20419-83 for technical ceramic products (subgroup 420-Celsius) and meet the requirements for modern radio-transparent ceramic materials.

References

[1] Dear P.S. (1957) Phase in system SrO – Al_2O_3 – SiO_2. Bull. Virginia Polytechn. Inst. № 11. P. 50.

[2] Shukla A. (2012) Development of a critically evaluated thermodynamic database for the systems containing alkaline-earth oxides. Genie metallurgique. № 1. 349 p.

[3] Y.-M. Sung, S. Kim. (2000). Sintering and crystallization of off-stoichiometric SrO–Al_2O_3–2SiO_2 glasses. Journal of Materials Science, Vol. 35, pp. 4293–4299.

[4] C. Ferone, B. Liguori, A. Marocco, S. Anaclerio, M. Pansini, C. Colella. (2010). Monoclinic (Ba, Sr)-celsian by thermal treatment of (Ba, Sr)-exchanged zeolite A. Microporous and Mesoporous Materials, Vol. 134, pp. 65–71.

[5] Y. Kobayashi, M. Inagaki. (2004). Preparation of reactive Sr-celsian powders by solid-state reaction and their sintering. Journal of the European Ceramic Society, Vol. 24, pp. 399-404.

[6] A. Marocco, B. Liguori, G. Dell'Agli, M. Pansini. (2011). Sintering behavior of celsian based ceramics obtained from the thermal conversion of (Ba, Sr)-exchanged zeolite A. Journal of the European Ceramic Society, Vol. 31, pp. 1965–1973

[7] P. Ptáček, F. Šoukal, T. Opravil, E. Bartoníčková, J. Wasserbauer. (2016). The formation of feldspar strontian ($SrAl_2Si_2O_8$) via ceramic route: Reaction mechanism, kinetics and thermodynamics of the process. Ceramics International, Vol. 42, № 7, pp. 8170-8178.

[8] Pat. 7867932 US, MPK C 03 C 10/0036. Refractory glass ceramics / George H. Beall; zayavnik I patentovlasnik Corning Inc. № 11/895847 zayavl. 28.08.2007; opubl. 05.03.2009.

[9] Pat. 5642868 US, MPK C 04 V 35/195. Ceramic material / Inna G. Talmy, Deborah A. Haught; zayavnik I patentovlasnik US Secretary of Navy. № 518604 zayavl. 02.05.1990; opubl. 01.07.1997.

[10] O. Zaichuk, A. Amelina, Yu. Hordieiev, Y. Kalishenko, N. Sribniak, S. Halushka, D. Borodai, A. Borodai. (2020). Patternsin the synthesis processes, the microstructure and properties of strontium anorthite ceramics modified by glass of spodumene composition. Eastern-European Journal of Enterprise Technologies, Vol 6. № 6 (108). p. 15 – 26. DOI: https://doi.org/10.15587/1729-4061.2020.216754

[11] Andreev, M. V., Drobakhin, O. O., Privalov, Y. N., Saltykov, D. Y. (2014). Measurement of dielectric material properties using coupled biconical resonators. Telecommunications and Radio Engineering, 73 (11), 1017–1032. doi: https://doi.org/10.1615/telecomradeng.v73.i11.70

[12] Yun Mo Sung, Kwak Woo Chul. (2002) Influence of Various Heating Procedures on the Sintered Density of Sr-celsian Glass-ceramic. Journal of Materials Science Letters. Vol. 21, № 11, pp. 841–843. https://doi.org/10.1023/A:1015710309425

[13] Yun Mo Sung. (2000) Monocelsian formation in the SrO–Al_2O_3–2SiO_2 glass. Journal of Materials Science Letters. Vol. 19, pp. 453–454. https://doi.org/10.1023/A:1006724930508

[14] Lisachuk G.V., Kryvobok R.V., Zakharov A.V., Chefranov E.V., Lapuzina O.M., Voloshchuk V.V., Samoilenko N.N. (2019) Technological parameters of ceramics creation on the basis of slawsonite. Éptőanyag - Journal of Silicate Based and Composite Materials. Vol. 71, № 2. pp. 48-53. https://doi.org/10.14382/epitoanyag-jsbcm.2019.9

[15] Lisachuk G.V., Kryvobok R.V., Zakharov A.V. et al. (2017) Optimization of the compositions area of radiotransparent ceramic in the SrO – Al_2O_3 – SiO_2 system. Przeglad Elektrotechniczny. Vol. 92, № 3., pp. 79–82. doi:10.15199/48.2017.03.19

[16] Lisachuk G.V., Kryvobok R.V., Fedorenko E.Y., Zakharov A.V. (2015) Ceramic radiotransparent materials on the basis of BaO-Al_2O_3-SiO_2 and SrO-Al_2O_3-SiO_2 systems. Építőanyag – Journal of Silicate Based and Composite Materials. Vol. 67, № 1., pp.20–23. http://dx.doi.org/10.14382/epitoanyag-jsbcm.2015.4

Ref.:
Lisachuk, G. V. – **Kryvobok**, R. V. – **Voloshchuk**, V. V. – **Lapuzina**, O. M.: *Investigation of the influence of temperature-time regimes on the morphological features of slawsonite ceramics*
Építőanyag – Journal of Silicate Based and Composite Materials, Vol. 74, No. 6 (2022), 224–228. p.
https://doi.org/10.14382/epitoanyag-jsbcm.2022.32

Composites of polyvinylpyrrolidone and polystyrene with rice husk ash as a bio and silica-rich material: thermal characteristics and water vapor absorption ability

Hamed NAZARPOUR-FARD
I was born in Iran, 1987. In the period of 2006–2010, I studied Applied Chemistry at Razi University, Kermanshah, Iran. Then, I received the Ms.C degree in Polymer Science on the topic of polymer composites from University of Isfahan (Iran) in 2012 and also the Ph.D degree in polymer Science from University of Guilan (Rasht, Iran), 2017. The sabbatical Leave was also passed at Iran Polymer and Petrochemical Institute (Tehran, Iran), 2016. Moreover, I have many reported papers and three published books in the polymer field. For more information, please refer the following web sites/pages.
The google Scholar Profile: https://scholar.google.com/citations?user=2J6TZnIAAAAJ&hl=en.
ORCID ID: 0000-0001-7177-8977

Hamed NAZARPOUR-FARD ▪ Department of Chemistry, Faculty of Sciences, Lorestan University, Khorramabad, Iran ▪ Nazarpour.ha@lu.ac.ir

Érkezett: 2022. 07. 06. ▪ Received: 06. 07. 2022. ▪ https://doi.org/10.14382/epitoanyag-jsbcm.2022.33

Abstract

The rice husk ash (RHA), which is bio-based and rich in the amorphous silica, was separately composited with polystyrene (PS) and K30 grade of polyvinylpyrrolidone (PVP) through the solution casting procedure. This bio- and natural-originated material was obtained from thermal pyrolysis of the rice husk (RH) at an elevated temperature. PS used in this study, was prepared by suspension radical polymerization and then the average molecular weight and polydispersity index for the synthesized PS were obtained via gel permeation chromatography. The pure polymers and the prepared bio-composites were characterized using X-ray diffraction (XRD) analysis and Fourier transform infrared (FT-IR) spectroscopy. Also, the effects of RHA on the XRD and FT-IR results were also studied. The thermal properties of these composites verified via thermogravimetry (TGA) analysis and differential thermal analysis (DTA), showed the enhancing effect of this additive on the thermal stability of the polymer matrices. In other word, the degradation temperatures of the polymers were enhanced as well as the increase of the final residual chars after incorporating the additive to the polymers that can be due to its good interactions and compatibility with these polymer matrices. Owing to the solubility of polyvinylpyrrolidone in water, some studies were performed on the hydrophilicity (water vapor absorption) of PVP and its composite. But, polystyrene due to its non-polar nature, didn't show the detectable ability in the water vapor absorption, so its hydrophilic characteristics were not additionally investigated. The results showed that the PVP-RHA bio-composite has the more hydrophobicity than the pure polyvinylpyrrolidone, which can be important in its usages, especially in the medical/pharmaceutical fields. Generally, RHA exhibited the good interactions with both PVP (the water-soluble material) and PS (the hydrophobic material) that can be attributed to the high diversity in the RHA components with the different polarities. RHA contains carbonic material, metal oxides, silica, silanol groups, etc.

Keywords: polyvinylpyrrolidone, polystyrene, rice husk ash, composite, thermal and hydrophobic features

Kulcsszavak: polyvinilpirrolidon, polisztirol, rizshéj hamu, kompozit, termikus és hidrofób tulajdonságok

1. Introduction

Polymer composites are the multi-component materials that are synthesized with the aim of modifying properties of various polymers and achieving the new characteristics and products [1-5]. The issues that accompany crude oil-based materials have encouraged many researchers to turn to biomaterials for different applications such as polymer composites. Polymer bio-composites in which at least one component is bio origin, are environmentally friendly and have benefits, e.g, renewability, non-toxicity, abundance and good availability. Among the bio-originated materials for this purpose, the residual material resulted from the industry of rice cultivation and production (i.e., both the cultivation and the post-harvest periods) as agricultural wastes can be used as the cheap and high-quality bio-additive. In rice mill industry, during the processing of the harvested rice, the large quantities of rice husk are produced. This material is the substantial environmental residue that can be converted into the proper materials with the high thermal stability, namely, rice husk ash by thermal decomposition protocol under the certain atmospheres and conditions [6-8].

Based on the review of the scientific literature, it was found that this bio-additive has been employed in many research studies. For example, rice husk ash has been exploited as the sustainable and the green biological waste for applications in renewable energy industries and building materials [6]. Also, in different cases, it has been studied as the convenient bio-sorbent for the removal of various pollutants such as toxic heavy metal ions from aqueous systems that the applicable results were obtained for the water treatment [9]. In addition to these examples, rice husk ash has been used in the structure of geopolymers to improve their desired traits [10]. Moreover, rice husk ash has been exploited as the suitable and inexpensive filler for the preparation of various polymeric composites [7, 8, 11 and 12], as well as its usages in highly efficient catalysts for using in organic chemical reactions [12-15].

Solution casting is the simple and the widely applied procedure in various research studies for the preparation of polymeric and other composites. For example, it has been employed to synthesize the efficient Nafion/mordenite composite membranes with the good permeability and the high uptake ability [16] and to prepare the superhydrophobic composite films [17].

Polystyrene which is soluble in non-polar solvents such as benzene and toluene, is the common polymer exploited in many usages and researches, e.g., the linear polystyrene films were synthesized via dissolving in the tetrahydrofuran/ethanol mixture and then evaporating with the aid of electricity for evaluating the effect of applied voltage on its characteristics [18]. Also, in another research work, a thin layer of polystyrene was created by casting the polystyrene solution in dimethylformamide under special conditions and then the light reflection features of the resulting films were studied [19].

Unlike polystyrene, polyvinylpyrrolidone is the water-soluble polymer that its composites are used in the bio-related fields, such as biomedicine. For instance, the films consisting of chitosan, polyvinylpyrrolidone and silver oxide nanoparticles were produced as the wound healing agents with the high antibacterial activity due to the presence of chitosan and silver oxide in their structure. Wound healing specifications of this substance was better than those of cotton, pure chitosan and other reported chitosan-based hemostatic dressings [20]. As well, polyvinylpyrrolidone/polyvinylbutyral composite has been applied as the stable binder for electrodes in supercapacitor structure that can be dispersed in aqueous electrolytes [21]. In another study, the palladium nanospheres stabilized on polyvinylpyrrolidone, were employed as the simple and new electrochemical sensor for amperometric detection of H_2O_2 [22].

It is expected that the rice husk ash can properly interact with both PS and PVP that are different together in polarity. This could be owing to the high diversity in the components present in RHA. This bio-material can react both chemically (e.g., by silanol groups (Si-O-H) with PVP) and physically (e.g., through the carbonic part of the bio-additive specially with PS that is the hydrophobic polymer) with these polymers. Van der Waals bondings are from the physical interactions that can be occurred between these polymers and the ash as an interfacial interplay.

It is noteworthy that after reviewing the literature, no article or the research work was reported on the thermal traits of RHA composites with polyvinylpyrrolidone and polystyrene. Based on the aforementioned ideas and the historical explanations, the main purpose of this paper was to prepare the PVP-RHA and PS-RHA composites by the solution casting technique and then to investigate the thermal properties of these materials. In addition, due to the importance of the polyvinylpyrrolidone hydrophilicity in some applications such as sutures, hemostatic materials (e.g., wound dressings) and other medical applications, the hydrophilicity of the PVP composite with RHA was also studied via evaluating the water vapor absorption by these composites.

2. Experimental

2.1 Materials

Polyvinylpyrrolidone (type K30) was purchased from Sobhan Pharmaceutical Company (Rasht, Iran). Polystyrene was synthesized by suspension polymerization method based on the published article [23]. The toluene sample used to dissolve polystyrene and to prepare the favorite solution of this polymer was produced by Merck chemical company. The rice husk studied in this study and its preparation procedure were the same ones as reported in [24]. Also, the rice husk ash was synthesized by pyrolysis of the prepared rice husk sample in a lab-scale furnace as previously reported [24].

2.2 Instrumentation

The process of sonication on the solutions was done using an ultrasonic bath (Sono Swiss, Sw3H, Switzerland). The gel permeation chromatography (GPC) was done via Knauer Instrument (Germany) for evaluating the average molecular weight and polydispersity index of the synthesized polystyrene. X-ray diffraction (XRD) measurements were performed on a Philips diffractometer (PW1840 made in Holland Netherlands) with Cu-Kα radiation. The Bruker Alpha FT-IR spectrometer was used to record the Fourier transform infrared (FT-IR) spectra using KBr disks. Thermogravimetric (TGA) analysis and differential thermal analysis (DTA) for investigating the thermal behaviors of the prepared samples were performed under the nitrogen atmosphere via Perkin-Elmer thermoanalyzer apparatus at the heating rate of 20 °C/min in the temperature range of 40 - 800 °C. The transformation of the rice husk to the favorite ash was accomplished by using a Nabertherm furnace (made in Germany) adjustable up to the temperature of 3000 °C. The moisture content of RH was removed via heating protocol via a drying oven (FN500P, NÜVE, Turkey).

2.3 Synthesis of polystyrene

The polystyrene sample used in this paper was synthesized via the suspension polymerization of styrene as the olefin monomer and benzoyl peroxide as the initiator of radical polymerization in a three-neck balloon under a nitrogen atmosphere and the certain conditions on the basis of the reported procedure carried out by Slobodian et al. [23]. The three-neck balloon was equipped with a mechanical stirrer to properly agitate the polymerization medium during the polymerizing the styrene monomer.

2.4 Preparing the rice husk and the rice husk ash

The rice husk (RH) was obtained by using the steps of milling, washing with distilled water, drying, smashing and then sieving by a stainless-steel sieve (200 mesh size), respectively, as reported in the previous study [24]. The rice husk ash was produced by burning the finely powdered rice husk at elevated temperatures as in [24].

2.5 Determining the solid and moisture content of the rice husk

The weight difference of the sample before and after the drying process at 110 °C for 1 h, was used for evaluating the moisture content of RH. And then, the percentage of the moisture trapped in the RH samples was computed by *Eq. (1)* [24].

$$\text{Moisture content of RH (\%)}: \frac{\text{Initial weight} - \text{Final weight}}{\text{Initial weight}} \cdot 100 \qquad (1)$$

To determine the solid residues of RH after pyrolysis, the given amount of the dried RH was put under the pyrolysis conditions at 600 °C for 1h and then the solid content of the RH sample after burning process was measured by *Eq. (2)* [24].

$$\text{RHA (\%)}: \frac{\text{Weight of dried RH} - \text{Weight of RHA}}{\text{Weight of dried RH}} \cdot 100 \qquad (2)$$

The more detailed information about the protocols used to determine the solid and moisture content of RH, have been reported in [24].

2.6 Preparing the PVP and PS composites with RHA

The uniformly powdered and sieved ash was added to the solution of PVP in the acidic distilled water along with the simultaneous stirring with a magnetic stirrer. The resulting mixture was agitated with the magnetic stirrer for 24 hours and then was placed in an ultrasonic bath for 20 min in order to the better dispersion of RHA in the solution. Finally, the well-dispersed ash in the aqueous PVP solution was poured into a glass plate and posited under the drying condition at 60 °C to prepare the final PVP-RHA composite. To synthesize the polystyrene composite, the uniform polystyrene solution in the toluene solvent was obtained at the ambient temperature. Then, by using the mechanical and ultrasonic agitation methods, the rice husk ash was uniformly dispersed in the polystyrene solution. Afterward, by evaporating toluene and drying the sample, the PS-RHA composite was synthesized for employing in the various desirable analyses.

2.7 Water vapor absorption tests

A simple method was applied to investigate the hydrophilicity of the PVP samples. In this experiment, the certain amounts (initial weight) of the polyvinylpyrrolidone samples was placed on a Whatman paper for the certain period of time and then incubated in the cylindrical chamber with the dimensions similar to *Fig. 1*. The chamber was then sealed for a convenient time at 25 °C and the water vapor absorbed by the samples during the period of incubation was evaluated by weighing the sample via *Eq. (3)*. At least 5 specimens of each sample were tested in this experiment and the average of the results was considered as the final result for the water vapor absorption of the sample. In all the hydrophilicity tests, the chamber contained 2 ml distilled water and the experiments were carried out in the ambient temperature and pressure.

$$\text{water vapor absorption (\%)} = \frac{\text{final weight} - \text{initial weight}}{\text{initial weight}} \cdot 100 \qquad (3)$$

In addition, the photographic method was employed to determine the amount of water vapor absorption by taking a picture of the wetted paper beneath the sample and evaluating the wetted area as the qualitative criterion of the absorbed water.

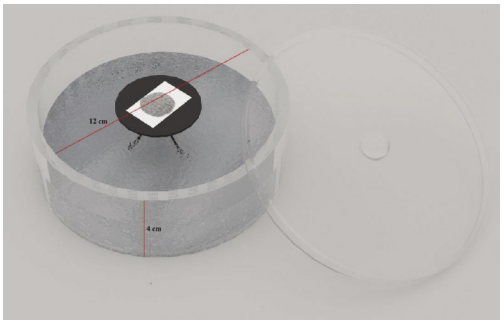

Fig. 1 The schematic representation of the chamber dimensions used in this study for testing the water vapor absorption by the PVP samples
1. ábra A PVP-minták vízgőzfelvételének vizsgálatához használt kamra méreteinek sematikus ábrázolása

3. Results and discussion

3.1 The compositions of RH and RHA

The main components of RH were observed to be silica, cellulose, lignin, hemicelluloses, soluble compounds and inorganic residue as reported in the previous study [24]. Moreover, the RHA composition was measured as L.O.I (12.70%), Al_2O_3 (0.25%), SiO_2 (80.82%), P_2O_5, (0.44%), SO_3 (0.39%), K_2O (1.25%), CaO (0.82%), Fe_2O_3 (0.38%), Cl (1.99%) and Na_2O (0.96%) by using X-ray fluorescence (XRF) analysis. The moisture content of the rice husk sample (8.2 ± 0.3 wt%) was found to be within the range of the reported values (8-15%). Also, the results exhibited that the RH weight loss during the pyrolysis process is 79.4 ± 1%, i.e., RH leaves 20.6 ± 1% of the solid residue (RHA) [24].

3.2 Gel permeation chromatography (GPC)

Gel permeation chromatography analysis was employed to determine the molecular weight and the molecular weight distribution (PDI) of the synthesized polystyrene. The results of this analysis were shown in *Fig. 2* and *Table 1*. As can be seen from these data, the weight and number average molecular weight values are 33949 and 19905 g mol^{-1}, respectively. The amount of molecular weight distribution for this prepared polymer was similar to that of the commercial polystyrene as reported in the literature [25].

Characteristic	Amplitude
Weight Average Molecular Weight	33949 g mol^{-1}
Number Average Molecular Weight	19905 g mol^{-1}
Z Average Molecular Weight	56512 g mol^{-1}
Z+1 Average Molecular Weight	84505 g mol^{-1}
Peak Molecular Weight	22409 g mol^{-1}
Polydispersity Index	1.705

Table 1 Average molecular weight and molecular weight distribution data for the synthesized polystyrene
1. táblázat A szintetizált polisztirol átlagos molekulatömege és molekulatömeg-eloszlása

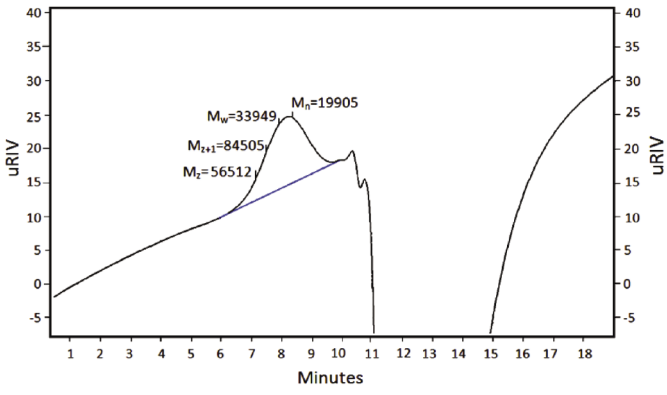

Fig. 2 GPC chromatogram for the synthesized polystyrene
2. ábra A szintetizált polisztirol GPC kromatogramja

3.3 X-ray diffraction (XRD)

Sample	Pos. [°2Th.]	Height [cts]	FWHM [°2Th.]	d [Å]	Rel. Int. [%]	Crystal size
PS	19.2	1084	1.3	4.6	100	1.2
PS-RHA	3.7	41.6	0.2	23.6	21.4	6.5
	5.3	34.8	0.2	16.56	17.9	7.9
	8.5	10.5	0.6	10.3	5.4	2.4
	11.1	8.6	2.5	7.9	4.4	0.6
	20.2	193	2.8	4.4	100	0.5
PVP	9.9	86.7	1.9	8.9	30.8	0.8
	23.0	281.0	1.0	3.9	100	1.5
PVP-RHA	3.4	14.3	2.8	26.2	7.6	0.5
	9.9	86.2	2.5	8.9	45.9	0.6
	11.6	111.7	1.2	7.6	59.4	1.2
	23.5	188	0.3	3.7	100	4.4

Table 2 Characteristics of the peaks observed in the XRD patterns
2. táblázat Az XRD mintákban megfigyelt csúcsok jellemzői

The crystallinity degree of the polymer composites as an essential factor determining the physical and mechanical differences between the composites and the parent polymers, was qualitatively investigated by XRD analysis. *Fig. 3* shows the XRD patterns of polystyrene, polyvinylpyrrolidone and their composites with the rice husk ash. The large and relatively narrow peak of polystyrene at 2θ around 20 indicate the semi-crystalline nature of polystyrene [26, 27] while the peaks of polyvinylpyrrolidone located at 2θ of 10 and 23 indicate the amorphous morphology for PVP [28]. It is obvious that the molecular arrangement and interactions between the composite components are of the main factors controlling the polymer crystallinity. According to *Table 2*, upon incorporating the filler to the polymer mortices, the polystyrene peak at 2θ of 19.2 was shifted to 20.2 and also d parameter accordance with this peak was decreased from 4.6 A° to 4.4 A° while its FWHM (full width at half maximum) was enhanced from 1.3° to 2.8°. the examples of peaks shift for PVP were 23.0° to 23.5°, 3.9 A° to 3.7 A° and 1° to 0.3° for 2θ, d-spacing and FWHM, respectively. These studies exhibited that upon adding the ash to these polymeric materials, FWHM and thereby the crystal size values of the samples are also changed, indicating the effect of RHA on the morphology of these polymers. It is noteworthy that, the intensity of the composite peaks was also significantly decreased as compared to the pure polymers. Moreover, the appearance of the new peaks in the patterns of the composites, exhibits the creation of the new crystalline area in the composites (*Table 2*). These changes occurred in the XRD patterns of PVP and PS after incorporating RHA into the polymer matrices, indicate the effective interfacial interplays between RHA and the polymers.

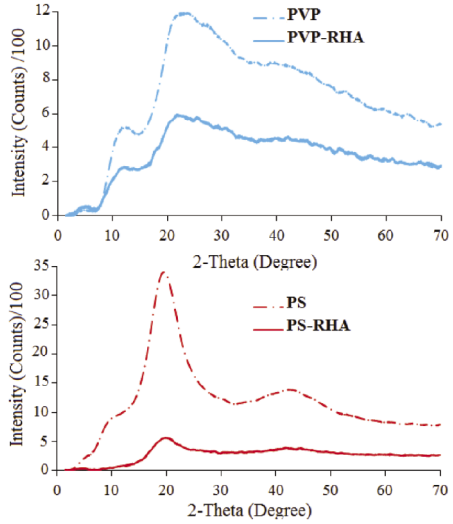

Fig. 3 XRD patterns of the samples
3. ábra A minták XRD eredményei

3.4 FT-IR spectroscopy

FT-IR analysis was performed to investigate the effect of the silica-rich rice husk ash on the polystyrene and polyvinylpyrrolidone vibrotational bands. The recorded FT-IR spectra of PS, PS-RHA, PVP and PVP-RHA can be observed in *Fig. 4*. In the case of polystyrene, the important peaks were occurred at around 3070-3000 cm^{-1} (the C–H stretching modes for the benzenoid ring), 2850-2920 cm^{-1} (the stretching modes of the saturated C–H bands) and 1596 cm^{-1} (assigned to the aromatic C=C bonds) [29]. The weak peaks at 1660 to 2000 cm^{-1} were attributed to the C-H bending mode of benzenoid rings while the ones at 1446 and 1490 cm^{-1} were related to the stretching vibration mode of the benzenoid rings framework. The bands appearing at around 757 and 695 cm^{-1} were also attributed to the C-H bending vibration mode of the benzenoid ring [30]. The peak at 3442 cm^{-1} could be related to the stretching vibration of O-H band due to the very small amounts of the absorbed water in the composite or to the peak overtone at 1721 cm^{-1}. It should be noted that the peak located at 3442 cm^{-1} was shifted to 3425 cm^{-1} wave number, which is the noticeable shift and can be due to the interactions and bonds between the silica-contained bio-additive and polystyrene structure. In other word, these interactions have been able to weaken the strength of these bonds thereby shift their stretching vibrations to the lower wave numbers as well as the significant decrement in their intensities.

In the case of polyvinylpyrrolidone, the C=O and C–N stretching modes were appeared at about 1654 and 1285 cm^{-1}, respectively. The results showed that the N and O atoms in PVP form the chemical bonds with SiO_2 existed in the rice husk ash,

which influenced on the coupling effect between C–O and C–N bonds [30-32]. The bands at 1014, 1222 and 1431 cm^{-1} were assigned to the CH_2 rocking, twisting and scissoring vibrations [26]. In addition, the wide band at 3452 cm^{-1} assigned to the O–H stretching vibration modes of the water molecules absorbed by the hydrophile polymer, was observably shifted to 3428 cm^{-1} while the band at 2142 cm^{-1} was objectively shifted to 2131 cm^{-1} wavenumber [32]. As well as these observable shifts to the lower wavenumbers, their intensities were also noticeably reduced. Additionally, a weak peak appearing at about 460 cm^{-1} could be due to the deformation of the Si-O bonds present in the RHA structure [33].

All these remarkable change in the peak wavenumbers and their intensities are the strong reasons for the presence of the good interactions between the components within the composites that have been able to cause such extensive and observable changes in most of the FT-IR peaks of these polymers. It is worthy of note that the RHA sample led to the similar effects on the FT-IR and XRD patterns of linear low density and high density polyethylenes [34].

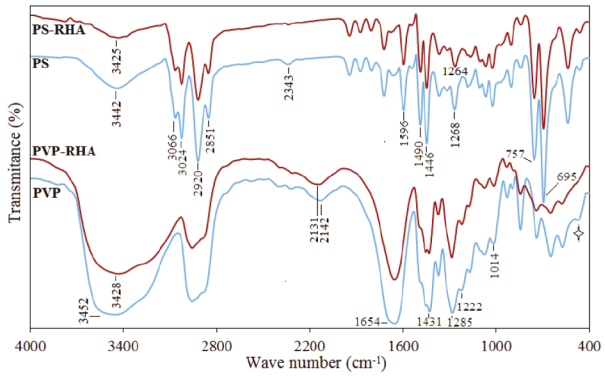

Fig. 4 IR spectra for the polymers and their composites
4. ábra A polimerek és kompozitjaik IR-spektrumai

3.5 Thermal properties

The thermal analysis is one of the most conventional and aplicabale experiments for studing polymeric materials. This analysis is very important because of the nesacary to improve the thermal stability of materials for various type of applications, especially when the material is subjected to the condition with the high temperatures, e.g., especial applications in aerospace and defense industries.

TGA/DTG and DTA analyses revealed that the thermal features of PS and PVP can be improved by incorporating the rice husk ash to them that is detailly explained in the following sections.

On the basis of *Fig. 5 (a)*, the initial weight losses equal 5% and 8% were appeared in the temperature range of 40-150 °C for PVP-RHA and PVP, respectively that is attributed to the elimination of the absorbed water. The peak starting at 350 °C and ending at around 500 °C is related to the decomposition temperature of PVP while the final weight loss starting at 500 °C is related to the combustion of organic residuals in the matrix [28]. As can be seen, the onset and offset temperatures of PVP degradation step have not significantly changed. However, in the themperature range of 450-600 °C, PVP-RHA exhibited 1-8.3% final char content more than that of PVP confirming the stabilizing effect of RHA on PVP. Additionally, no weight loss was observed above 675 °C for PVP-RHA and 710 °C for PVP which indicates the completion of the sample pyrolysis at these temperatures. This difference in the decomposition completion between two samples also implies the higher thermal stability of the composite as compared to pure PVP.

In the case of polystyrene (*Fig. 5 (b)*), it can be seen that polystyrene also decomposes in one step and its main degradation range is from 350 °C to about 450 °C that is consistent with the data reported in the literature [35]. As the stabilizing effect of silica on PS has been reported in literature [36], here, also the silica contained RHA enhanced the temperature in which polystyrene starts the degradation to the higher temperatures as compared to the pure polymer (*Fig. 5(b)*). Moreover, the composite has exhibited the higher residual char compared to the pure polystyrene indicating the stabilizing effect of the filler on the thermal stability of the polystyrene.

All the observed improvements in the degradation temperature and the higher residual char of the polymers at the elevated temperatures, can be attributed to the effective interfacial interactions between the polymers and RHA. Moreover, the ash undoubtedly has the high thermal stability that can lead to the enhancing influence on the thermal behavior of PS and PVP.

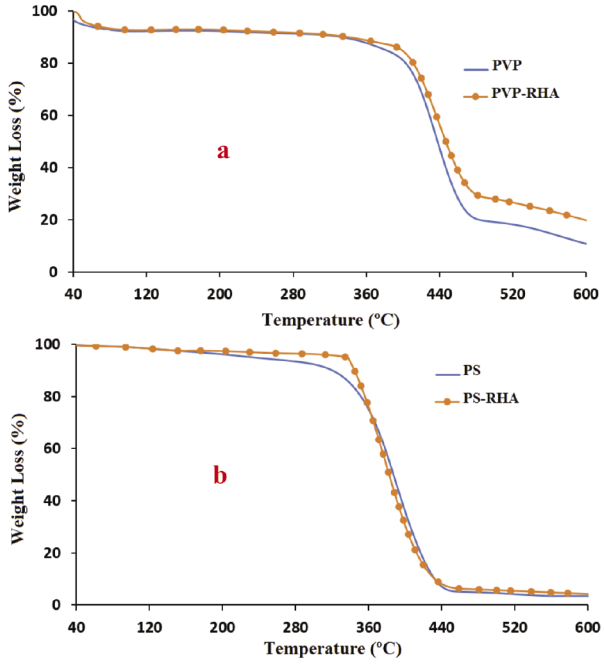

Fig. 5 TGA results of (a) PVP, PVP-RHA and (b) PS, PS-RHA
5. ábra TGA eredmények a) PVP, PVP-RHA és b) PS, PS-RHA

The results of DTA have been sumerized in *Fig. 6*. The endothermic peak appeared at about 100 °C, was related to the polyvinylpyrrolidone glass transition temperature (T_g) parameter. The broad endothermic peak at around 350 °C, is asigined to the thermal decomposition of the PVP samples acordance to the main thermal weight losses in TGA of PVP samples. The exothermic peaks at about 450 °C, are related to the thermal pyrolysis of the remaining residual organic

compounds. Also, the number of peaks observed for the pure polymer was greater than that of the composite (*Fig. 6*), i.e., the mechanism of the PVP thermal degradation is differ from that of PVP-RHA. It can be seen that the surface area under DTA curve of PVP-RHA composite is lower than that of the pure PVP that shows the less absorbed tharmal energy by the composite compared to the parent PVP (*Table 3*). This can be due to the fewer thermal events (such as degaradation and other thermally events or changes) in this sample and also to the stabilizing effect of RHA on the PVP thermal traits.

In the case of PS samples, similiar to PVP, the endothermic peak related to the Tg transition has appeard at 100 °C while the exothermic peak accordanc to the decomposition of PS has ocuured at the lower themperatures (around 300 °C) as compared to the PVP samples. Similarly, incorporating RHA to polystyrene affects the thermal stability of this polymer that led to the lower anergy absorbtion (the surface area under the sample curve) during the themperature elevation from the ambient temperature to ~750 °C (see *Table 3*).

The same reasons mentioned in the TGA section (the improved interfacial polymer/RHA interactions and the high thermal stability of RHA) can be employed for explaining the improving effects of RHA on the DTA results.

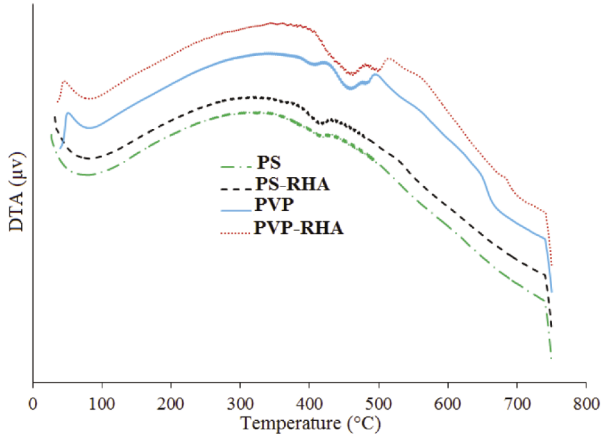

Fig. 6 Results of DTA analysis for the prepared samples
6. ábra Az előállított minták DTA-elemzésének eredményei

Sample	Surface area under the curves (μV °C) in the range of 100-600 °C
PS	4515
Ps-RHA	4036
PVP	4750
PVP-RHA	4325

Table 3 Comparison of the thermal energy absorbed by the samples
3. táblázat A minták által elnyelt hőenergia összehasonlítása

3.6 Hydrophilicity study of polyvinylpyrrolidone and its composite

It is clear that polyvinylpyrrolidone is the very hydrophilic and water-soluble polymer. In contact with moisture, this polymer absorbs the water molecules and its shape is converted from the powdery morphology to the lumpy/aggregated morphology. Maybe, for this reason, it has been employed in the hydrophilic drugs as the hydrogel [37]. Decreasing the PVP hydrophilicity could be the interesting aim for some usages of this polymer. For instance, the amount of water vapor absorbed by PVP-contained drugs has been previously studied [38]. Also, in other work the water vapor absorbed by PVP samples have been investigated that water vapor absorption was increased upon enhancing the relative humidity [39].

Here, the experimental results showed that the incorporation of the SiO_2-contained ash reduces the hydrophilicity of polyvinylpyrrolidone, according to which the water vapor absorption of polyvinylpyrrolidone composite was less than that of the pure PVP. This conclusion can be applicable/useful for the polyvinylpyrrolidone usages specially in some bio-applications that require the more hydrophobicity.

Also, the effect of the incubation time on the water vapor absorption was measured for the same amount (0.01 g) of the absorbent samples. The changes observed in the absorption values upon increasing the time can be seen in *Fig. 7*. Regardless of the difference in the amount of the water absorbed by the polymeric materials, the rate of water uptake by the samples was decreased after about 3 hours and reached its highest value after about 24 hours (*Fig. 7*).

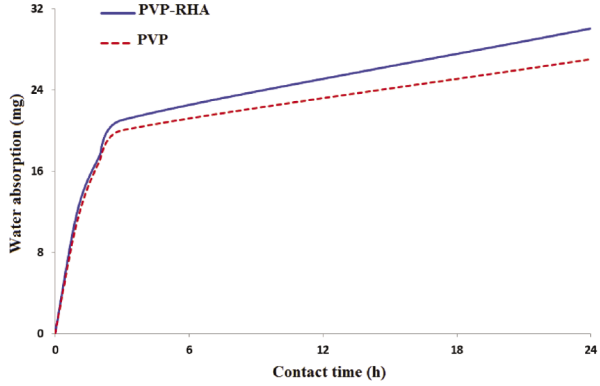

Fig. 7 Effect of the contact time (incubation time) on the water vapor absorption results
7. ábra A kontaktidő (inkubációs idő) hatása a vízgőz abszorpciójára

In other investigation, the effect of the initial weight (mass) of the absorbent on the water absorption parameter by the samples was evaluated and it was found that the water vapor absorption values of the samples increase upon increasing the amount of PVP and its composite. The trend of these changes (i.e., the changes occurred in the curve slope) can be seen in *Fig. 8*. This observation may be due to the fact that increasing the amount of absorbent leads to the increase of the number of water-absorbing sites at the sample surface.

Other experiment was comparison of the wetted area of the paper beneath the samples after hydrophilicity tests by incubation of the samples in the chamber. Comparing the circular wetted area can be the qualitative presentation of the amount of water absorbed by the PVP sample from the chamber environment (*Fig. 9*). This moist circular area around the sample on the paper is due to the water vapor trapped by the samples and then transferred to the paper below it. As can be seen in *Fig. 9*, the prepared composite exhibited the lower wetted area as compared to PVP due to its lower tendency for absorbing the water molecules than the pure polyvinylpyrrolidone.

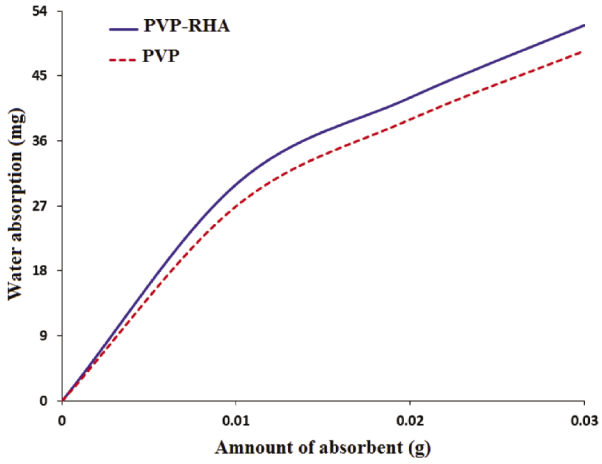

Fig. 8 Effect of the initial mass of the absorbent samples on the water vapor absorption results
8. ábra Az abszorbens minták kezdeti tömegének hatása a vízgőz abszorpciójára

A reasonable explanation for reducing the hydrophilicity of this polymer composite with RHA is the relatively strong bonds of polyvinylpyrrolidone with the bio-additives that are strong enough to reduce the dissolution of the composite in water. As shown in *Fig. 9*, the wetting area is uniform for polyvinylpyrrolidone because polyvinylpyrrolidone completely dissolves in water and uniformly penetrates into the paper. However, the image taken for the composite was seen as an irregular pattern due to the additive existence in its composition. The circles drawn on the papers after the test, are the areas in which water and the soluble polyvinylpyrrolidone have penetrated within the paper matrix, and the remaining dark stain from the composite can be related to the insoluble solid particles.

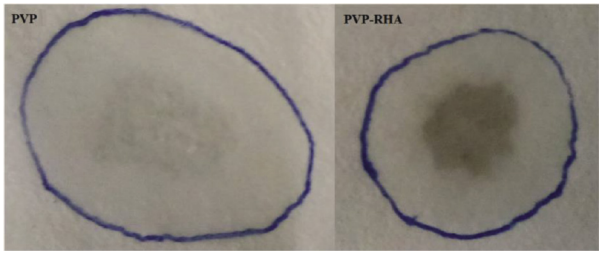

Fig. 9 The typical images taken from the wetted areas of the papers located beneath PVP and PVP-RHA, after the water vapor absorption test
9. ábra A PVP és PVP-RHA alatt található papírok nedvesített területeiről készült tipikus képek a vízgőzfelvétel vizsgálat után

4. Conclusion

In summary, this study showed that the rice husk ash can affect the XRD patterns of PS and PVP in the form of 2θ and intensity of the XRD peaks. Also, the FT-IR peak locations and intensities were also exhibited the changes after adding this bio-additive to the aforementioned polymers. Moreover, RHA led to enhancing the degradation temperature and the final residual solids (i.e., the thermal stability) of these polymers as observed in the TGA analysis. The DTA observations revealed the ~8.9% and ~10% decreases in the amount of the heat absorbed by PVP-RHA and PS-RHA, respectively during the elevation of temperature from ambient temperature to ~600 °C as compared to the parent samples. Moreover, after incorporating the rice husk ash to the PVP matrix, the degradation behavior and mechanism (the number of the peaks appeared in the DTA analysis) of this polymer was also changed. These observations can be attributed to the chemical structure of this bio-additive that contains more than 80% silica and the small proportions of metallic elements, and to its high thermal stability. Additionally, the water vapor absorption procedures exhibited the increasing effect of the rice husk ash on the PVP hydrophobicity after compositing it with this polymer matrix, which can be useful results for the bio-applications of this polymer. The fact that RHA have been capable to properly interact with both the hydrophilic PVP and the hydrophobic PS and to change their characteristics, could be ascribed to the high variety in the components of RHA. On the other word, this bio-material can react both chemically (e.g., via -Si-O-H groups with PVP) and physically (e.g., via the carbonic part specially with the nonpolar/hydrophobic PS as the interfacial interactions) with the polymers.

References

[1] Mirzajani, V., Nazarpour-Fard, H., Farhadi, K., Ghobadian, A. (2022). Copper Oxide Nano-Catalyst Incorporated TEGDN/NC/DAG Propellants: Thermal Behaviors and Kinetics. Propellants, Explosives, Pyrotechnics. e202100364. https://doi.org/10.1002/prep.202100364.

[2] Shamsi, R., Asghari, G. H., Mir Mohamad Sadeghi, G., Nazarpour-Fard, H. (2018) The effect of multiwalled carbon nanotube and crosslinking degree on creep–recovery behavior of PET waste originated-polyurethanes and their nanocomposites. Polymer Composites. Vol.39, No.S2, pp. E1013-E1024. https://doi.org/10.1002/pc.24420.

[3] Nazarpour-Fard, H., Rad-Moghadam, K., Shirini, F., Beheshty, M. H., Asghari, G. H. (2018) Reinforcement of epoxy resin/carbon fiber composites by carboxylated carbon nanotubes: a dynamic mechanical study. Polimery. Vo.63, No.4, pp.254-263. https://doi.org/10.14314/polimery.2018.4.1.

[4] Nazarpour-Fard, H., Behzadi-pour, G., Nasiri-Sarvi, M., Esmaili, P. (2019) PVA-based supercapacitors. Ionics. Vo.25, No.7, pp.2951-2963. https://doi.org/10.1007/s11581-019-03048-8.

[5] Behzadi-pour, G., Nazarpour-Fard, H., Fekri-aval, L., Esmaili, P. (2020) Polyvinylpyridine-based electrodes: sensors and electrochemical applications. Ionics. Vo.26, No.2, pp.549-563. https://doi.org/10.1007/s11581-019-03302-z.

[6] Akhter, F., Soomro, S. A., Jamali, A. R., Chandio, Z. A., Siddique, M., & Ahmed, M. (2021) Rice husk ash as green and sustainable biomass waste for construction and renewable energy applications: a review. Biomass Conversion and Biorefinery. pp.1-11. https://doi.org/10.1007/s13399-021-01527-5.

[7] Suhot, M. A., Hassan, M. Z., Aziz, S. A. A., Md-Daud, M. Y. (2021) Recent progress of rice husk reinforced polymer composites: A review. Polymers. Vol.13, No.15, pp.2391. https://doi.org/10.3390/polym13152391.

[8] Dutta, N., Bhadra, B., Gogoi, G., Maji, T. K. (2021) Development of polyvinyl chloride/waste rice husk ash/modified montmorillonite nanocomposite using epoxidized soybean oil as green additive substituting synthetic plasticizer and compatibiliser. Cleaner Materials. Vol. 2, pp.100033. https://doi.org/10.1016/j.clema.2021.100033.

[9] Priya, A. K., Yogeshwaran, V., Rajendran, S., Hoang, T. K., Soto-Moscoso, M., Ghfar, A. A., Bathula, C. (2022) Investigation of mechanism of heavy metals (Cr^{6+}, Pb^{2+} & Zn^{2+}) adsorption from aqueous medium using rice husk ash: kinetic and thermodynamic approach. Chemosphere. Vol.286, pp.131796. https://doi.org/10.1016/j.chemosphere.2021.131796.

[10] Hossain, S. S., Roy, P. K., Bae, C. J. (2021) Utilization of waste rice husk ash for sustainable geopolymer: A review. Construction and Building Materials. Vol.310, pp.125218. https://doi.org/10.1016/j.conbuildmat.2021.125218.

[11] Dutta, N., Maji, T. K. (2022) Development of waste rice husk/PVC/GO nanocomposite using TA–CaO adduct and ESO as green additives. Journal of Thermoplastic Composite Materials. 08927057211063398. https://doi.org/10.1177/08927057211063398.

[12] Flach, M. V., Krauspenhar, E., Jahno, V. D. (2022) Recycling of waste from the rice chain: incorporation of rice husk and rice husk ash in polymeric composites. Ciência e Natura. Vol.44, pp.e8-e8. https://doi.org/10.5902/2179460X68817.

[13] Bazani, H. A., Thomé, A., Affeldt, R. F., Probst, L. F. (2022) SBA-15 obtained from rice husk ashes wet-impregnated with metals (Al, Co, Ni) as efficient catalysts for 1, 4-dihydropyridine three-component reaction. New Journal of Chemistry. Vol.46, No.17, pp.7899-7909. https://doi.org/10.1039/D1NJ04835J.

[14] Teng, Z., Huang, S., Li, N., Zhou, Q. (2022) SO_2 Tolerance of Rice Hull Ash Based Fe-Cu Catalysts for Low-Temperature CO-SCR of NO. Catalysts. Vol.12, No.5, pp.534. https://doi.org/10.3390/catal12050534.

[15] Ngaini, Z., Jamil, N., Wahi, R., Shahrom, F. D., Ahmad, Z. A., Farooq, S. (2022) Convenient conversion of palm fatty acid distillate to biodiesel via rice husk ash catalyst. BioEnergy Research. Vol.15, No.2, pp.1316-1326. https://doi.org/10.1007/s12155-021-10331-y.

[16] Prapainainar, P., Theampetch, A., Kongkachuichay, P., Laosiripojana, N., Holmes, S. M., Prapainainar, C. (2015) Effect of solution casting temperature on properties of nafion composite membrane with surface modified mordenite for direct methanol fuel cell. Surface and Coatings Technology. Vol.271, pp.63-73. https://doi.org/10.1016/j.surfcoat.2015.01.021.

[17] Wen, X., Ye, C., Cai, Z., Xu, S., Pi, P., Cheng, J., Zhang, L., Qian, Y. (2015) Crosslinked superhydrophobic films fabricated by simply casting poly (methyl methacrylate-butyl acrylate-hydroxyethyl methacrylate)-b-poly (perfluorohexylethyl methacrylate) solution. Applied Surface Science. Vol.339, pp.109-115. https://doi.org/10.1016/j.apsusc.2015.02.077.

[18] Zhai, S., Zhi, Y. Y., Hu, E. J., Shen, Q. (2015) Formation of superhydrophobic polystyrene film by electric-assisted phase separation. Materials Letters, Vol.155, pp.54-57. https://doi.org/10.1016/j.matlet.2015.04.120.

[19] Xing, Z., Tay, S. W., Liu, Y., Hong, L. (2015) Solar heat reflective coating consisting of hierarchically assembled polystyrene nanoparticles. Surface and Coatings Technology, Vol.265, pp.99-105. https://doi.org/10.1016/j.surfcoat.2015.01.052.

[20] Archana, D., Singh, B. K., Dutta, J., Dutta, P. K. (2015) Chitosan-PVP-nano silver oxide wound dressing: in vitro and in vivo evaluation. International journal of biological macromolecules. Vol.73, pp.49-57. https://doi.org/10.1016/j.ijbiomac.2014.10.055.

[21] Aslan, M., Weingarth, D., Herbeck-Engel, P., Grobelsek, I., Presser, V. (2015) Polyvinylpyrrolidone/polyvinyl butyral composite as a stable binder for castable supercapacitor electrodes in aqueous electrolytes. Journal of Power Sources. Vol.279, pp.323-333. https://doi.org/10.1016/j.jpowsour.2014.12.151.

[22] Sophia, J., Muralidharan, G. (2015) Polyvinylpyrrolidone stabilized palladium nanospheres as simple and novel electrochemical sensor for amperometric hydrogen peroxide detection. Journal of Electroanalytical Chemistry. Vo.739, pp.115-121. https://doi.org/10.1016/j.jelechem.2014.12.021.

[23] Slobodian, P., Pavlínek, V., Lengálová, A., Sáha, P. (2009) Polystyrene/multi-wall carbon nanotube composites prepared by suspension polymerization and their electrorheological behavior. Current Applied Physics. Vol.9, No.1, pp.184-188. https://doi.org/10.1016/j.cap.2008.01.008.

[24] Nazarpour-Fard, H., Rad-Moghadam, K., Shirini, F., Beheshty, M. H. (2016) Novel improvements in thermal and hydrophobic properties of chitosan reinforced by rice husk ash. Polymers from Renewable Resources. Vol.7, No.4, pp.115-133. https://doi.org/10.1177/204124791600700401

[25] Chen, C. M., Hsieh, T. E., Ju, M. Y. (2009) Effects of polydispersity index and molecular weight on crystallization kinetics of syndiotactic polystyrene (sPS). Journal of alloys and compounds. Vol.480, No.2, pp.658-661. https://doi.org/10.1016/j.jallcom.2009.02.003.

[26] Xuemei, H., Hao, Y. (2013) Fabrication of polystyrene/detonation nanographite composite microspheres with the core/shell structure via pickering emulsion polymerization. Journal of Nanomaterials. 2013. https://doi.org/10.1155/2013/751497.

[27] Zhu, W., Wu, Y., Yan, C., Wang, C., Zhang, M., Wu, Z. (2013) Facile synthesis of mono-dispersed polystyrene (PS)/Ag composite microspheres via modified chemical reduction. Materials. Vol.6, No.12, pp.5625-5638. https://doi.org/10.3390/ma6125625.

[28] Sivaiah, K., Kumar, K. N., Naresh, V., Buddhudu, S. (2011) Structural and optical properties of Li^+: PVP&Ag+: PVP polymer films. Materials Sciences and Applications. Vol.2, No.11, pp.1688-1696. https://doi.org/10.4236/msa.2011.211225.

[29] Naim, A. A., Umar, A., Sanagi, M. M., Basaruddin, N. (2013) Chemical modification of chitin by grafting with polystyrene using ammonium persulfate initiator. Carbohydrate polymers. Vol.98, No.2, pp.1618-1623. https://doi.org/10.1016/j.carbpol.2013.07.054.

[30] Wang, D., An, J., Luo, Q., Li, X., Li, M. (2008) A convenient approach to synthesize stable silver nanoparticles and silver/polystyrene nanocomposite particles. Journal of applied polymer science. Vol.10, No.5, pp.3038-3046. https://doi.org/10.1002/app.28442.

[31] Abdelghany, A. M., Mekhail, M. S., Abdelrazek, E. M., Aboud, M. M. (2015) Combined DFT/FTIR structural studies of monodispersed PVP/Gold and silver nano particles. Journal of Alloys and Compounds. Vol.646, pp.326-332. https://doi.org/10.1016/j.jallcom.2015.05.262.

[32] Saravanan, L., Diwakar, S., Mohankumar, R., Pandurangan, A., Jayavel, R. (2011) Synthesis, structural and optical properties of PVP encapsulated CdS nanoparticles. Nanomaterials and Nanotechnology. Vol.1, pp.42-48. https://doi.org/10.5772/50959.

[33] Shirini, F., Akbari-Dadamahaleh, S., Mohammad-Khah, A. (2014) Rice Husk Ash: A New, Cheap, Efficient, and Reusable Reagent for the Protection of Alcohols, Phenols, Amines, and Thiols. Phosphorus, Sulfur, and Silicon and the Related Elements. Vol. 189, No.5, pp.577-586. https://doi.org/10.1080/10426507.2013.844142.

[34] Nazarpour-Fard, H. (2022) Rice husk ash: Economical and high-quality natural-based reinforcing filler for linear low-density and high-density polyethylene. Polymers from Renewable Resources. https://doi.org/10.1177/20412479221128965.

[35] Worzakowska, M. (2015) Thermal and mechanical properties of polystyrene modified with esters derivatives of 3-phenylprop-2-en-1-ol. Journal of Thermal Analysis and Calorimetry. Vol.121, No.1, pp.235-243. https://doi.org/10.1007/s10973-015-4547-7.

[36] Vaziri, H. S., Omaraei, I. A., Abadyan, M., Mortezaei, M., Yousefi, N. (2011) Thermophysical and rheological behavior of polystyrene/silica nanocomposites: Investigation of nanoparticle content. Materials & Design. Vol.32, No.(8-9), pp.4537-4542. https://doi.org/10.1016/j.matdes.2011.01.022.

[37] Bharali, D. J., Sahoo, S. K., Mozumdar, S., Maitra, A. (2003) Cross-linked polyvinylpyrrolidone nanoparticles: a potential carrier for hydrophilic drugs. Journal of Colloid and Interface Science. Vol.258, No.2, pp.415-423. https://doi.org/10.1016/S0021-9797(02)00099-1.

[38] Crowley, K. J., Zografi, G. (2002) Water vapor absorption into amorphous hydrophobic drug/poly (vinylpyrrolidone) dispersions. Journal of pharmaceutical sciences. Vol.91, No.10, pp.2150-2165. https://doi.org/10.1002/jps.10205.

[39] Teng, J., Bates, S., Engers, D. A., Leach, K., Schields, P., Yang, Y. (2010) Effect of water vapor sorption on local structure of poly (vinylpyrrolidone). Journal of pharmaceutical sciences. Vol.99, No.9, pp.3815-3825. https://doi.org/10.1002/jps.22204.

Ref.:
Nazarpour-Fard, Hamed: *Composites of polyvinylpyrrolidone and polystyrene with rice husk ash as a bio and silica-rich material: thermal characteristics and water vapor absorption ability*
Építőanyag – Journal of Silicate Based and Composite Materials, Vol. 74, No. 6 (2022), 229–236. p.
https://doi.org/10.14382/epitoanyag-jsbcm.2022.33

Phase composition and microstructure of ceramics made from kaolin mineral, alumina, and corn starch

Emese KUROVICS ▪ Institute of Ceramics and Polymer Engineering, University of Miskolc, Hungary ▪ fememese@uni-miskolc.hu
Jamal-Eldin F. M. IBRAHIM ▪ Institute of Ceramics and Polymer Engineering, University of Miskolc, Hungary
Mohammed TIHTIH ▪ Institute of Ceramics and Polymer Engineering, University of Miskolc, Hungary
Emese SEBE ▪ Institute of Ceramics and Polymer Engineering, University of Miskolc, Hungary
Érkezett: 2022. 09. 25. ▪ Received: 25. 09. 2022. ▪ https://doi.org/10.14382/epitoanyag-jsbcm.2022.34

Abstract
In this work, Sedlecky ml kaolinite, Nabalox No. 315 alumina and corn starch were used. The powder mixtures were milled and uniaxially pressed into pellets. Some properties of the raw materials and mixtures were investigated like TG, DTA, and the gas composition formed during the sintering process. The pellet samples were pre-sintered in the electric kiln under an oxygen-free reduction atmosphere at 1250 °C and then sintered in nitrogen gas at 1450 °C. The composition and microstructure of the produced specimens were tested.

The pyrolysis results show that in reducing pre-sintering 25 wt% of the mass of the corn additive remove from the ceramic body as gas. The remained part of the corn can incorporate into the material structure, and it may affect the further heat treatment processes. The mullite content of the ceramic samples increased from 43 wt% to 70 wt% because of high-temperature sintering in nitrogen gas. The mullite crystal structure has also changed. The increase in the amount of mullite phase is a consequence of the sintering process since the free SiO_2 and Al_2O_3 formed mullite crystals.
Keywords: alumina, free SiO_2, mullite, pyrolysis, sintering process
Kulcsszavak: alumínium-oxid, szabad SiO_2, mullit, pirolízis, szinterelési folyamat

Emese KUROVICS
is received her PhD degree in 2022 at the University of Miskolc. Where she is working as an assistant research fellow at the Institute of Ceramics and Polymer Engineering.

Jamal Eldin F. M. IBRAHIM
is a lecturer in the University of Bahri, Khartoum, Sudan, he graduated from University of Marmara, Istanbul, Turkey, Institute of Pure and Applied Sciences, Department of Metallurgical and Materials Engineering, for the time being, he is a PhD student in the University of Miskolc, Institute of Polymer and Ceramics Engineering, under supervision of Dr. István Kocserha.

Mohammed TIHTIH
is a lecturer in the Sidi Mohamed Ben Abdellah University, Morocco, he graduated from Faculty of sciences Dhar El Mahraz, Fez, Morocco, Department of Physics, for the time being, he is a PhD student in the University of Miskolc, Institute of Ceramics and Polymer Engineering, under supervision of Dr. István Kocserha.

Emese SEBE
is a PhD student at Institute of Energy and Quality, University of Miskolc, Hungary.

1. Introduction

Nowadays, a growing number of research works are carried out on the production of high-value-added products using waste or plant-origin renewable materials, which can also be observed in the case of research and development of new ceramic materials and products [1-14].

The authors in their previous works [15-19] have already shown the role of the plant origin additive in the production of ceramics. Usually, kaolin or zeolite rocks were used as raw minerals [17-19] because the goal was to produce ceramics with high mechanical strength using natural raw materials. The research and applications of clay-based composite materials have drawn a great deal of attention in recent years [20-22]. The mullite phase is formed during the thermal decomposition of clay minerals at above 1000 °C. During the sintering process of the ceramic products, different kiln atmospheres or temperatures can be used. Changing these parameters can produce different products with different properties. For example, the carbothermal reduction (CR) or the carbothermal reduction and nitridation (CRN) reactions of different clay minerals are well known. During the CR or CRN reactions, high-tech ceramic powders (SiC, Si_2ON_2, Si_3N_4, SiAlON) can be produced from traditional raw materials [20-27].

The authors have studied the possibilities of manufacturing advanced ceramics from traditional, relatively inexpensive raw materials and plant-origin additives by using the CR and CRN sintering processes.

2. Materials and experiments

During this research work, the authors used Sedlecky ml kaolin, Nabalox 315 alumina, and corn starch to make two mixtures. Corn starch was used as the carbon source additive that is necessary for the carbothermal processes. The composition of the mixtures was: mixture A – 90 wt% kaolin, 10 wt% alumina and mixture B – 64 wt% kaolin, 7 wt% alumina and 29 wt% corn starch. The raw materials were mixed in a planetary ball mill for 25 minutes at 150 rpm. Cylindrical samples were prepared with a diameter of 25 mm from the powder by the compression process. The pressed samples were first sintered at 1250 °C in a reduction atmosphere. This sintering method was partly the same as the carbothermal reduction, because of this the CR abridgment was used as a sign for the samples which were sintered in a reduction way. Later the samples were sintered at a higher temperature (1450 °C) using flowing nitrogen gas, like in the carbothermal reduction and nitridation process (CRN) of clay minerals. The use of higher amounts of corn starch in the described processes already significantly deteriorates the stability of the ceramic specimen during the heat treatment processes and therefore, in the present work was maximized the amount of corn starch to 29 wt%.

Before the heat treatments, the powders and mixtures were studied with a Derivatograph-C equipment to get the thermogravimetry (TG) and differential thermal

analysis (DTA) curves of the samples. In a pyrolysis study, the authors observed in advance the evolution of the gases during the heat treatment process in the case of the corn starch used, their evolution temperature, and the variation in the volume fraction of the gas components. In this way, for the carbothermic reactions important parameters were studied in advance: formation of CO and CO_2, residual liquid, and solid matter. The duration of the pyrolysis test was 2 hours using a heating rate of 10 °C/min. The test was performed in an electric tube furnace up to 900 °C. Composition of the formed gases was determined with a DANI 500 gas chromatograph.

The phase compositions of the sintered ceramics were determined by an X-ray diffractometer (XRD). To perform the phase composition analysis, the specimens were ground in a mortar into a sufficiently fine-grained powder. In this way, the average phase compositions were determined. The amorphous content was determined indirectly: the sum of all the crystalline phases considered to be 100% with the amorphous content. Test parameters: Cu Kα irradiation, accelerating voltage 40 kV, current 30 mA, step scanning mode, and the measurement range is 3-70° (2Θ). The microstructures were studied by Scanning Electron Microscopy (SEM) and Plasma-Focused-Ion-Beam Scanning Electron Microscopy (PFIB-SEM).

3. Results and discussions

In order to design the carbothermic reactions, the formation of CO and CO_2 gases was investigation in the case of corn starch additives. The specified total gas composition of the synthesis gas is summarized in *Table 1*, which clearly shows that the measured composition of the synthesis gas produced during the study is almost identical for the starch and mixture B (64 wt% kaolin, 7 wt% alumina and 29 wt% corn starch).

Tested samples	Gas composition, V/V%					
	CO_2	H_2	CO	CH_4	C_2-C_4	H_2S
Corn starch	32.91	31.58	23.23	10.31	1.97	<0.1
Mixture B	30.45	38.13	20.70	8.78	1.94	<0.1

Table 1 Total gas composition measured in the pyrolysis test
1. táblázat A pirolízisvizsgálat során mért teljes gázösszetétel

The study shows that combustible carbonaceous gases start to evolve, and volatile substances and hydrocarbons are released from the sample at temperatures above 350 °C in oxygen-depleted media (*Fig. 1*). In the test of the corn starch, more than 25 % of its original mass retained as pyrolysis coke and more than 50 % as pyrolysis oil. It shows that when using oxygen-depleted pre-sintering (CR), it expects that 25% of the mass of the plant additive (starch) will be removed from the ceramic samples as gas, and the remainder can incorporate into the material structure of the pre-sintered ceramic. Conversely, if this test was performed under conventional oxidation conditions, most of the starch would be removed as gas, as can be seen in the case of the thermogravimetry (TG) of the raw material (*Fig. 2*).

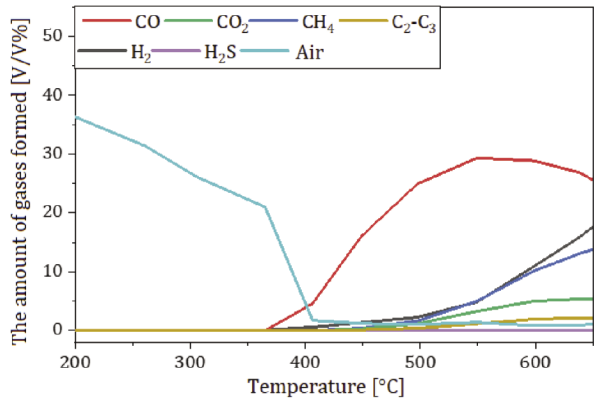

Fig. 1 Variation of gas composition during the pyrolysis test of corn starch
1. ábra A gázösszetétel változása a kukoricakeményítő pirolízisének vizsgálata során

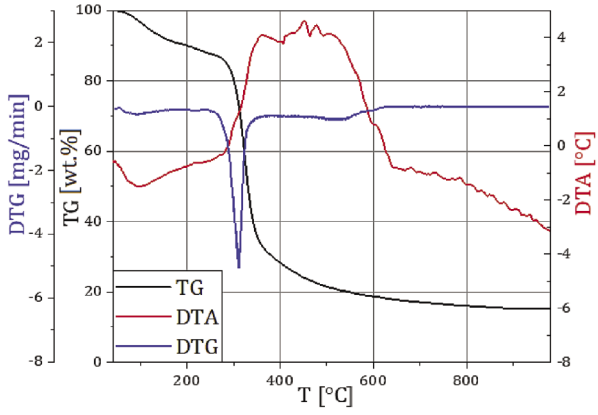

Fig. 2 Thermo-analytical curves of the corn starch
2. ábra A kukoricakeményítő termoanalitikai görbéi

After pyrolysis, the remaining high carbon content of the corn starch can play an important role as a carbon source during sintering in a nitrogen gas and can also contribute to the formation of a new pore structure during the second heat treatment (CRN sintering). The color of the samples changed depending on the used mixture and heat treatment (*Fig. 3*).

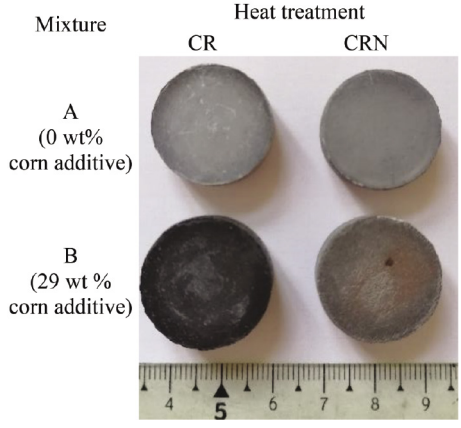

Fig. 3 The heat-treated samples
3. ábra A hőkezelt minták

As a result of CR sintering, the corn additive could not burn out from the ceramic matrix through the formation of CO or CO_2 gases. The skeletal structure of the corn particles remained in the ceramic body to increase the carbon content of the pre-

sintered (CR) samples (*Fig. 4*). This remained carbon content can help to incorporate nitrogen into the aluminosilicate ceramic structure [11].

The average results of the XRD measurements can be seen in *Table 2*. Based on the amount of phases, the mullite content of the ceramic samples increased from 43 wt% to 70 wt% as a result of high-temperature CRN sintering. The type of mullite transformed, and new mullite crystals formed by the reaction of free SiO_2 in the ceramic samples with the alumina, so the amount of mullite phase increased. The results show that a relatively high amorphous content was formed in the samples B (64 wt% kaolin, 7 wt% alumina and 29 wt% corn starch), while any nitrogen-containing crystalline phase was not detected. I.e., the residual carbon content from the corn starch proved to be insufficient to allow the formation of significant amounts of crystalline SiO_2N_2, Si_3N_4, or SiAlON phases in the material structure.

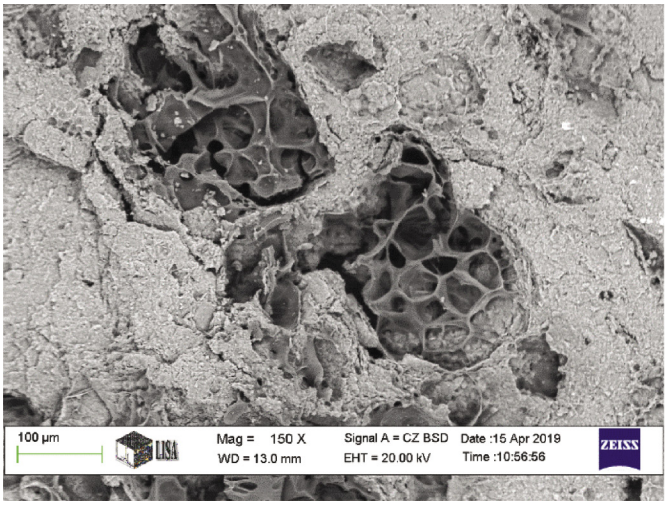

Fig. 4 The remained part of the corn starch in the ceramic body after sintering reduction atmosphere (CR)
4. ábra A kukoricakeményítő maradék része a kerámia testben a szinterezés után redukciós atmoszférában (CR)

Mixture sign (wt% corn)		A (0)		B (29)	
	Heat treatment	CR	CRN	CR	CRN
The detected phases, wt%	Amorphous	22	24	37	30
	Mullite	43	70	43	70
	Corundum	9	-	14	-
	Cristobalite	25	5.5	4	-
	Quartz	1	0.5	2	-

Table 2 The average phase compositions of the samples
2. táblázat A minták átlagos fázisösszetétele

The microstructure of the sintered samples shows needle-like mullite crystals with nanocrystals whose feature size is smaller than 200 nm. Large amount of amorphous phase which also includes these nanocrystals was stated by the X-ray measurement. Based on the PFIB-SEM studies of the sample B (64 wt% kaolin, 7 wt% alumina and 29 wt% corn starch) (*Fig. 5*), these nanocrystals are mullite crystals therefore the mullite content is even higher than the XRD results show.

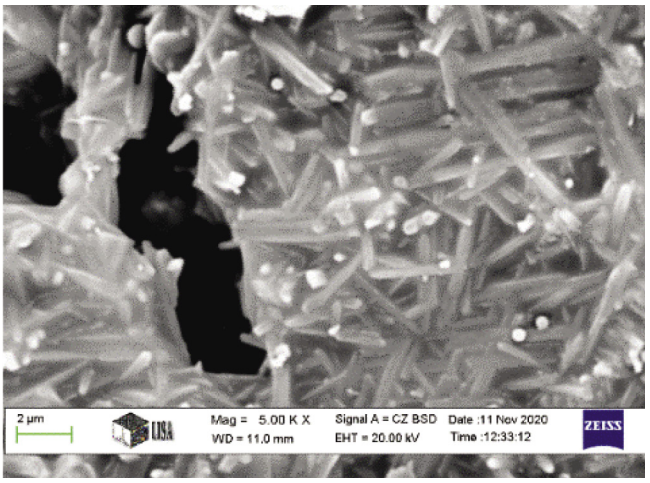

a)

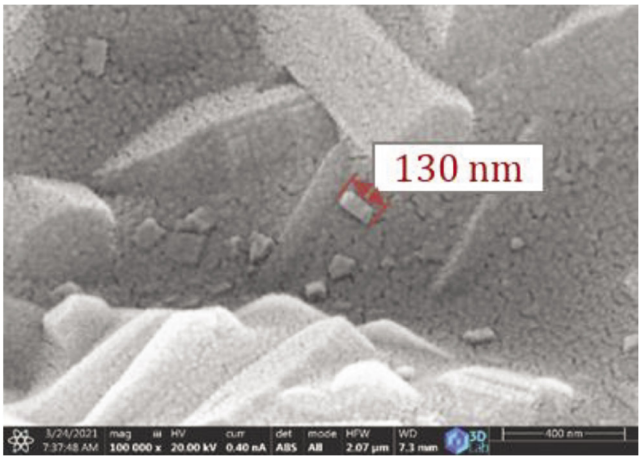

b)

Fig. 5 The microstructure of the CRN sintered sample B by SEM (a) and PFIB-SEM (b)
5. ábra A szinterezett B minta mikroszerkezete SEM (a) és PFIB-SEM (b) segítségével.

4. Conclusions

Based on the pyrolysis study of the reducing pre-sintering (CR) of ceramic samples containing corn starch additive, some part of the additive remained in the structure. 25% of the mass of the plant additive was removed from the ceramic samples in gaseous form, and the remained part can incorporate into the material structure. As a consequence, plant origin additive (corn starch) can play an important role as a carbon source and contribute to form new phase composition and to the formation of a different pore structure during the second heat treatment (CRN).

Based on the phase composition investigations it can be stated, that the mullite content of the ceramic samples increased during the CRN heat-treatment. Sintering at 1450 °C (CRN) changed the morphology of mullite particles from plates to needle-like crystals. The amount of mullite phase boosted from 43 wt% to 70 wt% by reason of high-temperature sintering in nitrogen gas (CRN). This way, mullite ceramics with higher purity were produced, compared with CR sintered specimens due to the amount of mullite phase increased by 27 wt%. This increase in the amount of mullite phase is a consequence of the sintering process since the free SiO_2 and Al_2O_3 were able to form mullite crystals.

Acknowledgement

The authors would like to say many thanks to IGREX Engineering Ltd for they support. They also thank their supervisor, Prof. Dr. László A. Gömze (1950-2022) for his encouragement and advice.

References

[1] G. Mucsi, Á. Debreczeni, V. Mádai, T. Dudok, B. Csőke 2011 Építőanyag 63 (1–2) 28–32. http://dx.doi.org/10.14382/epitoanyag-jsbcm.2011.6

[2] O. Fenyvesi, B. Jankus, Bence 2015 Építőanyag – JSBCM 67 (2) 66–70 http://dx.doi.org/10.14382/epitoanyag-jsbcm.2015.11

[3] B. Udvardi, K. Román, E. Kurovics, R. Géber, I. Kocserha 2019 WIT Transactions on Engineering Science 124 49-59. doi: 10.2495/MC190051

[4] A. Hamza, I. Kocserha, R. Géber, A. Buzimov 2019 IOP Conf. Series Materials Science and Engineering 613 012051 https://doi.org/10.1088/1757-899X/613/1/012051

[5] E. Kurovics, O.B. Kotova, L.A. Gömze, D.A. Shushkov, G.V. Ignatiev, P.A. Sitnikov, Y.I. Ryabkov, I.N. Vaseneva, L.N. Gömze 2019 Építőanyag – JSBCM, 71 (4) 114–119 https://doi.org/10.14382/epitoanyag-jsbcm.2019.20

[6] J.F.M. Ibrahim, E. Kurovics, M. Tihtih, P. Somdee, A.G. Gerezgiher, K. Nuilek, E.E. Khine, M. Sassi 2020 J. Phys.: Conf. Ser. 1527 012029 https://doi.org/10.1088/1742-6596/1527/1/012029

[7] M Sassi, J F M Ibrahim, A Simon 2020 J. Phys.: Conf. Ser. 1527 012037 https://doi.org/10.1088/1742-6596/1527/1/012037

[8] U. W. Robert et al. 2020 Építőanyag – JSBCM 72 (2) 72–78. https://doi.org/10.14382/epitoanyag-jsbcm.2020.12

[9] Flóra Asztalos and István Kocserha 2020 J. Phys.: Conf. Ser. 1527 012041 https://doi.org/10.1088/1742-6596/1527/1/012041

[10] OB Kolibaba et al 2020 J. Phys.: Conf. Ser. 1683 052012 https://doi.org/10.1088/1742-6596/1683/5/052012

[11] E Kurovics J F M Ibrahim, M Tihtih, B Udvardi, K Nuilek and L A Gömze 2020 J. Phys.: Conf. Ser. 1527 012034 https://doi.org/10.1088/1742-6596/1527/1/012034

[12] A. A. Akinwade et al 2021 IOP Conf. Ser.: Mater. Sci. Eng. 1107 012053 https://doi.org/10.1088/1757-899X/1107/1/012053

[13] E. E. Ambrose, F. O. Okafor, M. E. Onyia, 2021 Építőanyag – JSBCM 73 (3) 91–102. https://doi.org/10.14382/epitoanyag-jsbcm.2021.14

[14] Sassi, M.; Simon, A. 2022 Inorganics 10, 1. https://doi.org/10.3390/inorganics10010001

[15] E. Kurovics, L.A. Gömze, J.F.M. Ibrahim, L.N. Gömze 2019 IOP Conf. Ser.: Mater. Sci. Eng. 613 012025 https://doi.org/10.1088/1757-899X/613/1/012025

[16] E. Kurovics, A. Shmakova, B. Kanev, L.A. Gömze 2017 IOP Conf. Series: Materials Science and Engineering, 175 012013, http://dx.doi.org/10.1088/1757-899X/175/1/012013

[17] E. Kurovics et al. 2021 Építőanyag – JSBCM 73 (4) 149–153. https://doi.org/10.14382/epitoanyag-jsbcm.2021.22

[18] Ibrahim, Jamal Eldin F.M., Kotova, Olga B., Sun, Shiyong, Kurovics, Emese, Tihtih, Mohammed, and Gömze, László A., 2022 Journal of Building Engineering 45 103491

[19] E. Kurovics, B. Udvardi, K. Román, J. E. F. M. Ibrahim, L. A. Gömze 2019 WIT Transactions on Engineering Sciences 124 17 https://doi.org/10.2495/MC190021

[20] Li-Hua Xu, Fang Lian, Han Zhang, Yu-Bao Bi, Ke Cheng, Yang-Bao Qian 2004 Materials and Design 27 595–600 https://doi.org/10.1016/j.matdes.2004.12.017

[21] F.J. Narciso, F. Rodriguezreinoso 1994 Journal of Materials Chemistry, 4 1137-1141.

[22] X.-J. Liu, X.W. Sun, J.J. Zhang, X.P. Pu, Q.M. Ge, L.P. Huang 2003 Materials Research Bulletin. 38 1939–1948 https://doi.org/10.1016/j.materresbull.2003.09.018

[23] F. J. Li, T. Wakihara, J. Tatami, K. Komeya, T. Meguro 2007 Journal of the European Ceramic Society, 27 2535-2540.

[24] M.E. Bowden, K.J.D. MacKenzie, J.H. Johnston 1988 Materials Science Forum, 34-36 599-603. https://doi.org/10.4028/www.scientific.net/MSF.34-36.599

[25] Shuhai Jia 2005 Materials Science Forum 486-487 378-381. https://doi.org/10.4028/www.scientific.net/MSF.486-487.378

[26] Z. Tatlı, A. Demir, R. Yılmaz, F. Caliskan, Ali O. Kurt 2000 Journal of the European Ceramic Society 27. 743–747. https://doi.org/10.1016/j.jeurceramsoc.2006.04.062

[27] Zhibin Ma, Chaolu Wen, Kezhou Yan, Yanxia Guo, Fangqin Cheng 2019 Ceramics International 45. 22829–22840. https://doi.org/10.1016/j.ceramint.2019.07.325

Ref.:
Kurovics, Emese – **Ibrahim**, Jamal-Eldin F. M. – **Tihtih**, Mohammed – **Sebe**, Emese: *Phase composition and microstructure of ceramics made from kaolin mineral, alumina, and corn starch*
Építőanyag – Journal of Silicate Based and Composite Materials, Vol. 74, No. 6 (2022), 237–240. p.
https://doi.org/10.14382/epitoanyag-jsbcm.2022.34

GUIDELINE FOR AUTHORS

The manuscript must contain the followings: title; author's name, workplace, e-mail address; abstract, keywords; main text; acknowledgement (optional)**; references; figures, photos with notes; tables with notes; short biography** (information on the scientific works of the authors).

The full manuscript should not be more than 6 pages including figures, photos and tables. Settings of the word document are: 3 cm margin up and down, 2,5 cm margin left and right. Paper size: A4. Letter size 10 pt, type: Times New Roman. Lines: simple, justified.

TITLE, AUTHOR

The title of the article should be short and objective.

Under the title the name of the author(s), workplace, e-mail address.

If the text originally was a presentation or poster at a conference, it should be marked.

ABSTRACT, KEYWORDS

The abstract is a short summary of the manuscript, about a half page size. The author should give keywords to the text, which are the most important elements of the article.

MAIN TEXT

Contains: materials and experimental procedure (or something similar), results and discussion (or something similar), conclusions.

REFERENCES

References are marked with numbers, e.g. [6], and a bibliography is made by the reference's order. References should be provided together with the DOI if available.

Examples:

Journals:

[6] Mohamed, K. R. – El-Rashidy, Z. M. – Salama, A. A.: In vitro properties of nano-hydroxyapatite/chitosan biocomposites. *Ceramics International.* 37(8), December 2011, pp. 3265–3271, http://doi.org/10.1016/j.ceramint.2011.05.121

Books:

[6] Mehta, P. K. – Monteiro, P. J. M.: Concrete. Microstructure, properties, and materials. *McGraw-Hill*, 2006, 659 p.

FIGURES, TABLES

All drawings, diagrams and photos are figures. The **text should contain references to all figures and tables**. This shows the place of the figure in the text. Please send all the figures in attached files, and not as a part of the text. **All figures and tables should have a title**.

Authors are asked to submit color figures by submission. Black and white figures are suggested to be avoided, however, acceptable.

The figures should be: tiff, jpg or eps files, 300 dpi at least, photos are 600 dpi at least.

BIOGRAPHY

Max. 500 character size professional biography of the author(s).

CHECKING

The editing board checks the articles and informs the authors about suggested modifications. Since the author is responsible for the content of the article, the author is not liable to accept them.

CONTACT

Please send the manuscript in electronic format to the following e-mail address: femgomze@uni-miskolc.hu and epitoanyag@szte.org.hu or by post: Scientific Society of the Silicate Industry, Budapest, Bécsi út 122–124., H-1034, HUNGARY

We kindly ask the authors to give their e-mail address and phone number on behalf of the quick conciliation.

Építőanyag – *Journal of Silicate Based and Composite Materials*, Quarterly peer-reviewed periodical of the Hungarian Scientific Society of the Silicate Industry, SZTE.
http://epitoanyag.org.hu